Clim. Past Discuss., 7, 1511–1566, 2011
www.clim-past-discuss.net/7/1511/2011/
doi:10.5194/cpd-7-1511-2011

Climate of the Past Discussions

Hydrological variability in northern Levant over the past 250 ka

F. Gasse[1,**], **L. Vidal**[1], **A.-L. Develle**[1,*], **and E. Van Campo**[2]

[1]CEREGE, UMR6635, CNRS – (Aix-Marseille Université-CNRS-IRD-CdeF), BP 80, 13545 Aix-en-Provence cedex 04, France
[2]ECOLAB, UMR5245, (CNRS-Université de Toulouse-INPT), BP 24349, 31062 Toulouse cedex 9, France
[*]now at: Laboratoire Chrono-Environnement, UMR6249, CNRS – Université de Franche-Comté, 16 Route de Gray, 25030, Besançon cedex, France

[**] *Invited contribution by F. Gasse, recipient of the EGU Hans Oeschger Medal 2010.*

Received: 13 April 2011 – Accepted: 14 April 2011 – Published: 10 May 2011

Correspondence to: F. Gasse (gasse@cerege.fr)

Published by Copernicus Publications on behalf of the European Geosciences Union.

Abstract

The Levant features sharp climatic gradients from North to South and from West to East resulting in a large environmental diversity. The lack of long-term record from the northern Levant limits our understanding of the regional response to glacial-interglacial boundary conditions in this key area. The 250 ka paleoenvironmental reconstruction presented here is a first step to fill this geographical gap.

The record comes from a 36 m lacustrine-palustrine sequence cored in the small intra-mountainous karstic basin of Yammoûneh (northern Lebanon). The paper combines times series of sediment properties, paleovegetation, and carbonate oxygen isotopes, to yield a comprehensive view of paleohydrologic-paleoclimatic fluctuations in the basin over the two last glacial-interglacial cycles. Efficient moisture was higher than today during interglacial peaks around 240, 215–220, ~130–120 ka and 11–9 ka (although under different Precipitation minus Evaporation balance). Moderate wetting events took place around 170, 150, 105–100, 85–75, 60–55 and 35 ka. The penultimate glacial period was generally wetter than the last glacial stage. Local aridity culminated from the LGM to 15 ka, possibly linked to water storage as ice in the surrounding highlands. An overall decrease in local water availability is observed from the profile base to top. Fluctuations in available water seem to be primarily governed by changes in local summer insolation controlled by the orbital eccentricity modulated by the precession cycle, and by changes in precipitation and temperature seasonality.

Our record is roughly consistent with long-term climatic fluctuations in northeastern Mediterranean lands, except during the penultimate glacial phase. It shares some features with speleothem records of western Israel. Conversely, after 130 ka, it is clearly out of phase with hydrological changes in the Dead Sea basin. Potential causes of these spatial heterogeneities, e.g., changes in atmospheric circulation, regional topographic patterns, site-specific climatic and hydrological factors, are discussed.

CPD
7, 1511–1566, 2011

1 Introduction

The Levant (Fig. 1), which extends from Southeast Turkey to northern Egypt and Arabia, is a key area to study climatic changes at the transition between the temperate Mediterranean domain and the subtropical belt of the Saharan-Arabian desert. Moisture in the region primarily comes from the eastern Mediterranean Sea (EMS). Rainfall decreases with latitude, and more sharply from W to E with distance from the seashore and because mountain ranges running parallel to the coastline intercept a large part of the precipitation coming from the West. Altitudes range from ~425 m below sea level (b.s.l.) along the Dead Sea shore to more than 3000 m above sea level (a.s.l.) in Lebanon. This unique physiogeographic pattern results in a large diversity of environmental conditions which vary dramatically over short distances. Numerous geological and archeological data show that the Levant has experienced huge climatic fluctuations and a long history of human evolution during the Late Quaternary. Changes in water availability may have played a major role in the early modern humans migration out of Africa and in the Pleistocene-Holocene cultural dynamics of Eurasia (Bar-Yosef, 1998; Vaks et al., 2007; Shea, 2008; Carto et al., 2009; Waldmann et al., 2010; Frumkin et al., 2011). However, a North-South disparity in data coverage limits our understanding of the response of the whole Levantine region to global climatic changes and of the relationships between societal evolution and climates.

In central and southern Levant (Israel mainly), intensive paleoenvironmental studies have provided well-dated, long-term, high resolution records. In the rain-shadow of the Judean mountains, lake level fluctuations and periods of speleothem growth/non deposition in the Dead Sea basin demonstrate generally high effective moisture attributed to enhanced rainfall during glacial phases, and dry conditions during Interglacials (see the recent reviews by Enzel et al., 2008; Waldmann et al., 2010; Frumkin et al., 2011). Long-term $\delta^{18}O$ fluctuations in continental carbonates in the Levant are primarily driven by the glacial/interglacial variations in the isotopic composition of the moisture source (the EMS surface water) (Frumkin et al., 1999; Bar-Matthews et al., 2003; Kolodny et

CPD
7, 1511–1566, 2011

al., 2005). However, rainfall amount is probably the second order factor that modulates $\delta^{18}O$ changes, and has likely increased in western Israel during Interglacials (Bar-Matthews et al., 2003; Almogi-Labin et al., 2009; Frumkin et al., 2011). In the southern Negev desert, only sporadic wet pulses have occurred and were possibly associated with intrusions of humidity from southern sources during interglacial periods (Vaks et al., 2010; Waldmann et al., 2010).

In northern Levant (Lebanon, northern Syria and SE Turkey), no record spans the last climatic cycles. The few available records (≤21 ka) show a large early Holocene wetting followed by a desiccation trend after 7–6 ka (Yasuda et al., 2000; Verheyden et al., 2008; Hajar et al., 2008, 2010; Develle et al., 2010). Northward, long-term pollen, lake and speleothem records from northeastern Mediterranean regions to western Iran (Lézine et al., 2010; Tzedakis et al., 1994, 2009; Djamali et al., 2008; Badertscher et al., 2011) reflect generally warm-wetter interglacial and cold-drier glacial environments related to temperature and ice sheet waxing/waning in higher latitudes of the Northern Hemisphere (NH), but hydrologically out of phase with the Dead Sea basin evolution.

New data are needed to decipher whether climatic changes well recorded in the southern Levant have also affected the northern Levant, and understand how the whole region has responded to the North Atlantic-Mediterranean system and to southern influences.

The present paper provides a long multiproxy paleoenvironmental record for the northern Levant. It derives from a lacustrine sediment sequence collected in the small karstic basin of Lebanon (Yammoûneh, Fig. 1), and spans approximately the past 250 ka. The sequence has already been analyzed for chronological purposes and sedimentary processes (Develle, 2010; Develle et al., 2011), carbonate oxygen isotopes (only the past 21 ka; Develle et al., 2010), and paleovegetation (Van Campo et al., unpublished). Major results are briefly summarized below. In addition, we present new $\delta^{18}O$ data spanning the last 250 ka. Our aim here is to combine time series from individual indicators to yield a comprehensive view of environmental fluctuations in the basin over the two last glacial-interglacial cycles. An attempt is made to disentangle

CPD
7, 1511–1566, 2011

the role of local versus regional and global climate factors by comparison with other environmental records from surrounding regions. We discuss the potential causes that might explain spatial similarities and disparities in the hydrological evolution of the Levant.

2 Modern setting

2.1 Main physiogeographic features of the Levant region

The steep topography of the Levant is related to the active Levant Fault System (Le Pichon and Gaulier, 1988) that runs from the NW tip of the Red Sea to SE Turkey. East of narrow coastal plains, SSW-NNE mountain ranges create an orographic barrier, rising up to 3083 m a.s.l. in Mount Lebanon at only 20–25 km from the sea shore. Just eastward, a chain of deep tectonic basins stretches along the Levant Fault (from south to North, the Arava valley, the Dead Sea and Tiberias lake basins along the Jordan Valley, and the Ghab Valley in Syria; Fig. 1). Regional climate is primarily controlled by the Mediterranean cyclonic systems related to the North Atlantic system, but distance from the seashore and the complex orography strongly modulate the regional and local rainfall pattern.

The Levant experiences a Mediterranean climate with wet cool winter and warm dry summer. Winter precipitation is generated by the cyclonic activity over the Sea (Sharon and Kutiel, 1986), when the Siberian anticyclone is reinforced over SW Asia and the Azores High extends over North Africa and Spain (Fig. 2a, b). The Mediterranean cyclogenesis is influenced by the surrounding regions and possibly by long distance teleconnections, e.g., the North Atlantic Oscillation (NAO) (Ziv et al., 2006, 2010; Dayan et al., 2008; Raible et al., 2010). Cyclones, either generated in the Mediterranean basin or penetrating from the North Atlantic, are steered by the mid-latidude westerlies and tend to propagate eastward along the northern coast of the Mediterranean until reaching the Levant region. When propagating over the relatively warm seawater, air

CPD
7, 1511–1566, 2011

masses become saturated by moisture. In the EMS, polar intrusions create a deep upper-level trough accompanied by low-level cyclogenesis. The strength and position of cyclones formed or reactivated in the EMS (the Cyprus Lows, Fig. 2a) largely control the winter rainfall temporal and spatial variability in the Levant (Enzel et al., 2003; Ziv et al., 2006). In summer (Fig. 2c, d), when the Siberian anticyclone is attenuated and the Azores anticyclone and the mid-latitude westerly belt are shifted northward, the Levantine region is warm and dry. The summer low-pressure systems developed southward and eastward (the Red Sea Trough and the Persian Trough) are generally hot and dry (Kahana et al., 2002).

Several mechanisms indirectly relate the Levant to subtropical and tropical climates. Very dry summer conditions over the eastern Mediterranean region and northeastern Sahara are partly due to the subsidence of easterly airflows linked to the Indian monsoon activity (Rodwell and Hopkins, 1996; Ziv et al., 2004). Most of the occasional rainfalls occurring in the Negev desert during spring and autumn are in conjunction with an active Red Sea Trough extending from East Africa through the Red Sea (Kahana et al., 2002). Heavy dust storms of North African origin are frequent from December to April. Saharan dust influx to the region has often been attributed to the thermal lows of the Sharav cyclones formed over Libya and Egypt (Alpert and Ziv, 1989) and the Red Sea through, but the cold Cyprus Lows also play a major role in attracting Saharan dust plumes (Dayan et al., 2008). The Nile River discharge, which depends on tropical rainfall in Ethiopian highlands and equatorial East Africa, affects the EMS hydrothermal dynamics (Rossignol-Strick and Paterne, 1999) and thus sea-land interactions.

2.2 The Yammoûneh basin in Lebanon

The Yammoûneh basin (34.06° N–34.09° N, 36.0° E–36.03° E, 1360 m a.s.l.), 6 km long, 2 km wide, lies at approximately 37 km from the sea shore on the eastern flank of Mount Lebanon (Fig. 3). The basin is today entirely cultivated. It was occupied in its southern part by a seasonal lake from at least Roman times to the 1930's when it was drained for irrigation of the Bakka plain. No paleo-shoreline was observed,

CPD
7, 1511–1566, 2011

suggesting that the paleolake never reached high levels during a period long enough to leave geomorphic evidence. The basin is a SSW-NNE depression of tectonic origin along the Yammoûneh Fault, a segment of the Levant Fault System. It was downfaulted through thick sub-tabular sequence of intensively karstified Cenomanian dolomitic limestones (Dubertret, 1975; Hakim, 1985). The strike-slip Yammoûneh Fault is active (slip rate: 3.8–6.4 mm yr^{-1}) but vertical movements likely remained negligible during the Late Quaternary (Daëron et al., 2004, 2005, 2007; Elias, personal communication, 2009). Westward, the Yammoûneh basin is limited by the high Mnaïtra plateau that abruptly rises to 2100 m a.s.l. To the East, gently sloping hills (Jabal el-Qalaa, 1500 m a.s.l.) separates the Yammoûneh basin and the large Bakka plain synclinal.

In Lebanon (Service Météorologique du Liban, 1977; Karam, 2002), mean Annual Precipitation (MAP) ranges from 700–1000 mm along the coast, >1400 mm in Mount Lebanon, to 400 mm in the Bakka plain and <200 mm in the NE. Above 2000 m a.s.l., precipitation is essentially niveous. At Yammoûneh, MAP reaches 900–1000 mm, as snow falls over about 30 days yr^{-1}. The wet-cold season (November–March) culminates in January, while precipitation are almost nil from June to August. Continentality is marked by large diurnal and seasonal variations in temperature and air humidity. Mean Annual Temperature (MAT) is about 15 °C but freezing occurs over 3 months yr^{-1} and temperature maximum largely exceeds 30 °C during the warmest month (July).

The strong rainfall and temperature gradients in Lebanon result in natural vegetation belts ranging from forest and woodland to open steppe (Abi-Saleh and Safi, 1988). From the seashore upward, the western slopes of Mount Lebanon present a transition from successive Mediterranean, montane to subalpine vegetation zones characterized by different arboreal taxa reflecting the altitudinal rainfall and temperature gradients (Table 1). In the drier environments of the eastern flank of Mount Lebanon, only xerophytic Mediterranean trees (evergreen oaks) and subalpine junipers are present (Table 1). The Bakka plain is open to influx of steppe elements from the adjacent eastward regions. Human impact has considerably deteriorated and modified the natural ecosystems since millenia.

CPD
7, 1511–1566, 2011

Hydrologically, the Yammoûneh basin primarily depends on precipitation over the western highlands. Direct precipitation on the paleolake surface (<1.2.10^6 m^3 yr^{-1}) and on the small surface watershed (~105 km^2; Develle et al., 2011) is negligible compared to the important water inflow brought by permanent karstic springs (35–70.10^6 m^3 yr^{-1}; Besançon, 1968; Hakim, 1985). Beneath the Mnaïtra plateau, subterranean karstic networks collect snowmelt water feeding a dozen springs along the western edge of the basin. The cool karstic spring water exhibits an isotopic composition (mean: $\delta^{18}O = \sim -8.9‰$, $\delta D = \sim -50.8‰$) very close to that of winter rainfall (~90 % of MAP), δ_P, in the watershed (Develle et al., 2010), without significant impact of evaporation or sublimation before infiltration (Aouad et al., 2004). Studies of nearby karstic aquifer systems show that groundwater residence time is negligible on the geological time-scale (from 1 season to 2–3 yr; Aouad et al., 2005; El Hakim, 2005). Following the smooth slope of the basin, sinuous channels drain spring and runoff water from the west into karstic sinkholes along the opposite eastern border. The karstified, intensively fissured and faulted basin floor is highly permeable. Hence, the basin is hydrologically open with rapid throughflow despite the absence of surface outlet. Residence time may have, however, increased when a permanent lake occupied the basin.

3 Material, methods and results on individual proxies

3.1 Material

The present paper deals with the upper 36 m of the longest sediment core (YAM-04C', 73 m) collected in 2004 from the central part of the Yammoûneh paleolake, apart of the Yammoûneh Fault disturbances localised by geoelectric profiles (Sursock and Gasse, 2005) and two trenches dug throughout the fault (TR01, 5 m deep, 75 m-long; TR02, 9.5 m-deep, 50 m-long; Daëron, 2005; Daëron et al., 2007).

Trenches and cores have revealed a thick (≥73 m), sub-continuous accumulation of lacustrine-palustrine sediments. The definition of stratigraphical units and sub-units

CPD
7, 1511–1566, 2011

was based on macroscopic descriptions at core opening (sediment color, texture, main components) and smear slide observations. A very simplified stratigraphic log of the upper 36 m of core YAM-04C' and pictures of some core sections illustrate the variety of lithofacies (Fig. 4) described in details in Develle et al. (2011).

Schematically, the profile shows two main types of sediments, although transitions between stratigraphic units are often gradual:

i. pale intervals, a few meters thick, dominated by carbonates. They consist of whitish powdery silt or very fine sand (Units I, thicker in trenches than in the core, VI and IX; Fig. 4e) rich in calcified rests of aquatic organisms (gastropods, ostracods, charophytes, fish otoliths...), or of light gray to light brown marl (Unit IV and part of Unit IX; Fig. 4c).

ii. thick accumulations of intensively colored silty clay. This siliciclastic material is almost devoid of shells (besides ostracods). The ocher to reddish brown Unit II (Fig. 4b) shows numerous strongly oxidized, indurated layers and beds of coarse limestone gravels and concretions. Units III, V, VII and VIII consist of plastic olive gray (Fig. 4d) or grayish brown silty clay (Fig. 4f) often organized in bands 2–20 cm thick. Lighter marly intervals are interbedded in these units. Several layers, 3–8 cm thick, suggest paleosoils (e.g., around 2240, 2165, 1615, 1600, 930 cm) and a few centimetric intervals are laminated.

The lowest carbonate-rich Unit X (Fig. 4g) differs from others by its very dark brownish to black color and its peaty feature. It contains abundant aquatic plant fragments, beds of fish otoliths and of well-preserved mollusc shells. Below 3650 cm, it overlays greenish clays resembling Units III or VIII.

Superimposed to these first order subdivisions, subtle changes in color and texture occur at the centimetric to millimetric scale. All encountered remains of aquatic organisms are typical of fresh, shallow or even ephemeral waterbodies.

Analyses performed on the core for environmental reconstruction are listed in Table 2.

CPD
7, 1511–1566, 2011

3.2 Major analytical results

3.2.1 Chronological framework

The construction of an age model of core YAM-04C' (Develle, 2010; Develle et al., 2010, 2011) was based on the combination of radiometric dating and magnetic chronostratigraphy. The position of dated levels along the profile is showed Fig. 4a.

The upper part of the sequence was ^{14}C-dated. Radiocarbon ages were obtained by Accelerator Mass Spectrometry (AMS) from wood fragments collected in the trenches and in the core, stratigraphically correlated using remarkable lithofacies, magnetic susceptibility and δ^{18}O ostracod profiles. The ^{14}C ages were calibrated using IntCal 09 (Reimer et al., 2009). Eleven levels are ^{14}C-dated from 0–20 ka for the upper ~250 cm. The ^{14}C age at 535 cm (47 ± 4 ka) is doubtful as it reaches the limit of the ^{14}C method applicability. One level of almost pure authigenic calcite has provided a reliable U/Th age of 124 ± 17 ka at the depth of 1770 cm. Measurements of magnetic parameters allowed us to identify four geomagnetic events (1 to 4; Fig. 4a) based on changes in inclination and relative paleointensity of the Earth magnetic field. The very well identified Event 2 (1590–1660 cm) is the Blake event (~114–120 ka). Events 1 and 3 may represent the Laschamp (41 ± 2 ka, 340–370 cm, peaking at 361 cm) and the Iceland Basin event (~190–194 ka; 2735 cm), respectively. Event 4 (3420–3490 cm) coincides either with the Pringle Falls event (~211 ka) or the Mamaku event (230 ± 12 ka). An approximate age of 230 (+12/−20) ka was assigned at 3460 cm.

Between the above mentioned age control points, the age-depth relationships were estimated by linear interpolation. Units are tentatively related to the stacked and orbitally-tuned Marine Isotope Stages (MIS; Martinson et al., 1987). We are aware that the Develle et al. (2011) age model only provides an approximate time scale, due to the low number of dated points, age uncertainties, changes in sedimentation rate, and possible sedimentation hiatuses. Nevertheless, ^{14}C ages clearly show that Unit I (truncated at ~7.5 ka in the core) is of Holocene age (MIS 1). According to the U/Th date and the depth position of the geomagnetic Blake event, Unit VI is assigned with

CPD
7, 1511–1566, 2011

confidence to the last Interglacial peak, MIS 5.5. If the age proposed for geomagnetic event 4 is correct, Unit IX represents MIS 7, a hypothesis supported by its lithofacies analogies with Units I and VI. An attempt to improve our age model, assuming that vegetation and lithofacies changes are controlled by local summer insolation, is proposed below (Sect. 4.1).

3.2.2 Paleovegetation

Most of the sedimentary sequence contains pollen grains, although its top (<8.3 ka) is sterile possibly due to oxidation after the lake drainage (as the post-glacial part of trench TR02). Vegetation patterns were inferred from the pollen record, based on 225 samples (Van Campo, unpublished). The percentages of major pollen taxa are plotted vs. depth Fig. 5.

Abundant aquatic and subaquatic plant pollen indicates the occurrence of a permanent waterbody and marshes or wetlands around the core site, respectively. Terrestrial pollen taxa or taxa groups (Table 1) reflect the development of: (i) cold wet forests from the subalpine (*Juniperus*) and montane belts (*Cedrus* and *Abies*); (ii) temperate wet climate of the upper Mediterranean zone (deciduous *Quercus*); (iii) mesic forests from the Middle Mediterranean zone (*Pinus* and evergreen *Quercus*) supporting warm and dry summers; (iv) steppic-desertic landscapes (*Artemisia* and Chenopodiaceae). Cichorioideae pollen, which resists oxidizing conditions and frequent desiccations (as observed in stratigraphic Unit II), is placed within this last group. The total percentage of tree pollen (AP %) provides a broad view of the alternance between forested and steppic landscape, mainly attributed to changes from moist to drier conditions.

Major points arising from the pollen study are the following:

CPD
7, 1511–1566, 2011

Arboreal vegetation dominates during interglacial optimums, early-mid MIS 7, MIS 5.5 and early MIS 1, which were wetter/warmer than today. These phases coincide with different arboreal pollen types. MIS 7 (maximum AP %) is characterized by peaks of junipers alternating with deciduous oaks and by the highest occurrence of aquatic plant pollen, indicating high Precipitation (P) and/or low Evaporation (E) under relatively cool conditions. Mesic Mediterranean conditions predominant during MIS 5.5 reflect a lower ($P - E$) balance than during MIS 7. Temperate deciduous oaks prevailed during the early Holocene.

MIS 6 shows a step-wise moisture increase. After a steppic stage, cool-wet coniferous forest elements become abundant, and aquatic-subaquatic plant pollen indicates, by times, high local water availability.

From MIS 5.5 to the LGM, an overall trend towards arid conditions is punctuated by wet pulses of decreasing amplitude. These pulses are recorded by peaks of Mediterranean trees tentatively assigned to MIS 5.3 around 1500 cm (~100–105 ka) and MIS 5.1 at 1150–960 cm (~85–73 ka), and two subsequent events during the last glacial period around 750 cm (~65–60 ka) and 500 cm (~45 ka). Effective moisture after the MIS 5.5 onset remained, however, too low or too unstable for the development of aquatic/subaquatic plants or for their pollen preservation in the sediments. Clearly, the last glacial phase was generally drier than MIS 6.

The driest intervals (minimum AP %) fall during the LGM and the last deglaciation, and at the MIS 7/6 transition.

3.2.3 The sedimentary record

Methods, main analytical results (Fig. 6) and discussion on sedimentary processes are presented in Develle (2010) and Develle et al. (2011). Main conclusions are summarized below.

Sedimentation has been primarily controlled by: (i) in situ lacustrine carbonate production, (ii) erosion of the surface watershed, and (iii) eolian inputs.

CPD
7, 1511–1566, 2011

The whitish Units I, VI and IX coincide with interglacial periods (MIS 7, MIS 5.5, MIS 1). They mainly consist of calcite precipitated into the waterbody (authigenic rhomboedric crystals and biogenic fragments). Lacustrine calcite production was enhanced by high temperature, strong biological activity in the lake, and high Ca^{2+} inputs suggesting heavy karstic spring discharge and active circulation in the Mnaïtra karstic system. Arboreal vegetation in the basin limited runoff-derived detrital inputs and favored carbonate dissolution through percolation of soil humic acids. Low magnetic susceptibility values (K_{LF}) as well as relatively low contents of Fe, Ti and K and TOM, were attributed to reduced local erosion and dilution of detrital particles by authigenic carbonates. The quasi-absence of runoff-derived material could be interpreted as very low rainfall, but active groundwater inflow, the synchrony of the carbonate and tree pollen (AP %) peaks, and the abundance of lacustrine organims rather suggest high water availability in both the aquifer recharge area and the Yammoûneh basin.

Colored clayey silts are mainly composed of local terrigenous and eolian material. Lithofacies, which include paleosoils, and the scarcity of aquatic organisms (mainly ostracod taxa able to survive ephemeral conditions) generally reflect shallow, unstable palustral environments. Calcite, present throughout, generally occurs in aggregates resembling those found in watershed soils or as limestone gravels, indicating its detrital origin. Dolomite is also probably eroded from the bedrock. Elements other than Ca generally prevail and are supported by minerals of detrital origin responsible for high K_{LF} values. Clay minerals (smectite mainly, kaolinite, traces of illite) are attributed to weathering and runoff in the basin, indicating at least occasional heavy floods. Quartz, K-feldspars and plagioclases, almost absent in the local bedrock, are obviously allochtonous and windblown from remote sources. Quartz (up to 60 %), largely dominates the non-carbonated fraction, reflecting a high contribution of eolian dust to sedimentation.

Marls (Unit IV and IX) and pale marly layers interbedded in silty clay are intermediate between these two typical sediment types. The peaty marl of Unit X, rich in TOM and biogenic rests, indicates the occurrence of a productive lake at the core site.

CPD
7, 1511–1566, 2011

3.2.4 The carbonate oxygen isotope record

The carbonate $\delta^{18}O$ record (Fig. 7) was obtained from ostracod valves, common and well preserved in most samples. Analyses were performed on 190 levels using the 4 most abundant taxa (*Ilyocypris inermis, I. gibba, Candona neglecta* frequent in Unit I), and *Fabaeformiscandona balatonica* (only present below 1800 cm), following the same procedure as Develle et al. (2010). Interspecific $\delta^{18}O$ differences were determined, all values were normalized to the most widespread taxon (*I. inermis*) and corrected for the vital effect (~2.4‰) estimated for this species (Develle et al., 2010). This correction provides values coeval with that of authigenic calcite (δ_c) which would have precipitated at equilibrium in the same ambient water. Toward the top, the Yammoûneh δ_c record includes some levels from the trench TR02 where the whole Holocene period is represented.

The δ_c fluctuations of continental carbonates reflect complex interactions between several climatic variables and site-specific factors (see references in Develle et al., 2010). Calcite $\delta^{18}O$ values are primarily controlled by water temperature and isotopic composition of the ambient water, here lake water (δ_L). The δ_L values are governed by the isotopic composition of the water inflow (δ_{in}) and of other terms of the lake water balance (inflow – [Evaporation + outflow]). The term δ_{in} depends on the precipitation $\delta^{18}O$ values (δ_P) and the P-E balance in the lake catchment. The δ_P values are in turn controlled by the isotopic composition of the moisture source, here that of EMS surface water (δ_{sw}), storm-track trajectories, and the negative/positive relationships with local rainfall amount and ground-temperature.

Along the 250 ka Yammoûneh profile, δ_c values fluctuate by 5.1‰, between −12.6 and −7.5‰ (Fig. 7a). The profile is characterized by δ_c values generally lower before MIS 5.5 suggesting overall wetter conditions than later, a reverse δ_c trend between MIS 6 and the last glacial period, and very sharp δ_c rises during interglacial peaks.

Factors controlling δ_c over the past ~21 ka were discussed in Develle et al. (2010). First, δ_L was estimated by correcting δ_c for lake water temperature, using the few

CPD
7, 1511–1566, 2011

available data on regional paleotemperatures. Second, isotopic composition of the moisture source (δ_{sw}) was derived from planktonic foraminifera (*G. ruber*) $\delta^{18}O$ records (δ_{foram}) in a Levantine core (MD84-632, Fig. 1; Essalami et al., 2007), corrected for surface water temperature using alkenone-based SST (SST_{alk}) records from the same core. Thirdly, the difference $\Delta^{18}O = \delta_{sw} - \delta_L$ was calculated in order to discuss the impact of the "source effect" on the Yammoûneh isotopic signal. The authors concluded that both the "source effect", amplified by increase inland rainfall during the early Holocene, and the large glacial-interglacial temperature changes have been important drivers on $\delta^{18}O$ fluctuations. Changes in storm-track trajectories may have also contributed to the signal.

The same approach is attempted here to interpret major glacial/interglacial δ_c changes over the past 250 ka, but should be regarded with great caution because of large uncertainties on timing and marine data used to reconstruct δ_{sw} and δ_L. We used time series of δ_{foram} from the high resolution core MD-9501 (86 ka; Almogi-Labin et al., 2009) and the poorly-resolved record of ODP 967 from Kroon et al. (1998) complemented by detailed measurements focused around sapropel events (Emeis et al., 2003) (Fig. 7b). Although not recorded in SPECMAP (Imbrie et al., 1984), δ_{foram} fluctuations between 180 and 130 ka of the same amplitude as in ODP 967 were observed in cores 84MD-648 and −637 (Fig. 1) closer to the Nile delta (Ducassou et al., 2007). SST_{alk} records from the eastern EMS either do not extent over the last 250 ka (Essalami et al, 2007; Castañeda et al., 2010) or are discontinuous (core ODP 967; Emeis et al., 2003). We used the SST_{alk} record of core MD40-71 from the northwestern boundary of the Levantine basin (Emeis et al., 2003; Fig. 7c) as a rough regional indicator of temperature deviations relative to modern, ΔT, at sea level ($\Delta T_{sealevel}$). By combining the δ_{foram} and the $\Delta T_{sealevel}$ values, we applied the paleotemperature equation of Craig and Gordon (1965) to infer an approximate record of δ_{sw} for the northern Levantine basin (Fig. 7d).

At Yammoûneh, we assume that the water temperature of the shallow waterbody was in equilibrium with air temperature. In the Levant, inland quantitative paleotemperature

CPD
7, 1511–1566, 2011

estimates prior to the LGM are limited to sporadic data inferred from isotope geochemistry of Soreq Cave speleothems (McGarry al., 2004, Fig. 7b; Affeq et al., 2008) between 140 ka and present. EMS SST_{alk} can serve as a first-order approximation of land paleotemperatures for Levantine inland temperature (Bar-Matthews et al., 2003), at least at Soreq. The temperature effect was taken into account by using EMS $\Delta T_{sealevel}$ data to infer ΔT at Yammoûneh (ΔT_{Yam}) to correct δ_c for lake water temperature with the same paleotemperature equation as for δ_{sw} to obtain δ_L (Fig. 7e). During Interglacials, we assume that the mean annual temperature difference between sea level and Yammoûneh was the same as today. For full glacial periods, the thermal atmospheric lapse rate was steepened, by at least 2 °C km^{-1} during the LGM in the Mediterranean domain (Kuhlemann et al., 2008). Permanent glaciers on the western flank of Mt Lebanon evidenced by moraines above 2000 m a.s.l. (likely from LGM age according to preliminary ^{36}Cl ages) also attest for an enhanced thermal gradient (L. Benedetti, personal communication, 2010). An additional cooling of 2.5 °C at Yammoûneh and ≥4 °C in the aquifer recharge zone (>2000 m a.s.l.) would have induced an additional decrease of δ_L of ~0.7‰ (water temperature effect), but a larger decrease of δ_P values of ~ −1.4 to at least −2.3‰ due to the "ground-temperature effect" (estimated at ~0.58‰/°C in northern mid-latitudes; Rozanski et al., 1993) reducing the $\delta_L - \delta_P$ difference (Fig. 7e). Because most of the precipitation was likely niveous (more depleted than liquid rainfall, Rozanski, 2005), δ_P may have decreased even more.

The "source effect" is extracted by calculating $\Delta\delta^{18}O = \delta_{sw} - \delta_L$ (Fig. 7f). Large $\Delta\delta^{18}O$ variations indicate that other factors than the "source effect" have acted on δ_L and δ_c. During Interglacials, low $\Delta\delta^{18}O$ values compared to the modern $\delta_{sw} - \delta_P$ difference (~ −11‰) likely reflect enhanced inland rainfall around 220 and 125–120 ka and less clearly around 105, 85–75 ka and 11–9 ka (Fig. 7f). The $\Delta\delta^{18}O$ decreases are associated with remarkable rises of δ_c and δ_L particularly clear at ~126–120 or ~85–75 ka. Several hypotheses can be invoked to explain these apparent discrepancies. First, increased δ_P, due to changes in either rainfall seasonality or air mass trajectories, may have occurred, increasing δ_L, and thus decreasing $\Delta\delta^{18}O$. At Yammoûneh,

CPD
7, 1511–1566, 2011

modern winter ^{18}O-precipitation values are lower than spring and autumn values by ~2.5‰ (Develle et al., 2010). The transition to higher δ_L and lower $\Delta\delta^{18}O$ values could reflect a longer rainy season, increasing the relative contribution of spring and fall precipitation on the mean annual δ_P values. Presently, at the rainfall event scale, the less ^{18}O-depleted rains close to Beirut (δ_P: −2 to −4‰) are associated with air masses from the North (Aouad et al., 2004, 2005). Enhanced advection of northerly winds might have increased δ_P. Second, amplified seasonal thermal contrasts, as expected from increased summer insolation, would have induced ^{18}O-enrichment of δ_{in} through evaporation during dry seasons warmer than today when a lake or wetlands maintained all year-round at the core site.

During Glacials, low δ_c, δ_L and δ_p values (Fig. 7f) suggest the dominance of ^{18}O-depleted winter rains and primarily reflect the effects of low water- and atmospheric-temperatures. The $\Delta\delta^{18}O$ values fluctuate around the δ_{sw}– δ_p values inferred for full glacial times, as expected from the source effect, but sharp negative peaks suggest wet pulses at ~170 ka and 150–145 ka and during short MIS 4–3 intervals. Freezing over most of the year have likely inhibited evaporative ^{18}O concentration. Changes in storm tracking may have contributed to the isotopic signal. Today, the most ^{18}O-depleted rains reaching Lebanon (δ_P:−6 to −11‰) come directly from the west and have a long path over the sea (Aouad et al., 2004–2005). Major storm-tracks funneled along the southern EMS coast due to ice extent in northern high latitudes, as proposed by Enzel et al. (2008), may have enhanced the δ_P decrease and $\Delta\delta^{18}O$ increase.

Our approach suggests that the isotope balance of the Yammoûneh hydrosystem was initially controlled by the “source effect” (δ_{sw}), but this first order factor was modulated and modified by the “amount effect”, local water and ground temperature changes, and modifications of the atmospheric circulation system.

CPD
7, 1511–1566, 2011

3.2.5 Relationships between environmental indicators

A Principal Component Analysis (PCA; using the Analyseries 2.0 software, Paillard et al., 1996) integrating primary (rough) data from different environmental indicators provides a broad overview of the relationships between them. The PCA includes 21 proxies (variables) listed in Table 2. These variables were reconstructed with different depth/time resolution and along different core length. Therefore, data were re-sampled with a common depth scale between 3360 and 64 cm, although this procedure looses information for high resolution proxies and shortens the record. The matrix used in the PCA finally consists in 157 core levels and 21 environmental variables translated into standard deviation units. Table 3 shows the coefficients of simple linear correlations between these variables. The 3 first PCA principal components represent 72 % of the total variance (PC1: 48.1 %; PC2: 14.3 %; PC3: 9.5 %). The PC1 and PC2 scores and the projection of the variables in factorial plans F1-F2 and F1-F3 are plotted in Fig. 8.

PC1 scores confirm the 2 poles of sediment components, carbonate vs. all other components, already highlighted by Develle et al. (2011). Axis 1 is strongly and positively loaded by elements and minerals of obvious detrital origin, magnetic susceptibility and colored silty-clay facies. Ca and calcite (+aragonite) contents are the major contributors on the negative side. Axis 1 also opposes the steppe pollen assemblage, associated with detrital elements, to all other pollen groups placed on the Ca side.

PC2 differentiates the lower (below ~1800 cm) and upper halves of the sequence. This asymmetry is largely due to the strong positive loading on Axis 2 of pollen from cool-wet conifer forests and aquatic-subaquatic biotopes (better developed in the lower part) and the negative loading of δ_c values (generally lower before MIS 5.5 and opposed to all tree pollen). Axis 3 is also mainly defined by pollen assemblages and δ_c. Interestingly, the ordination of pollen groups along Axis 3 reflects a gradient in available moisture and temperature: the strongest PC3 positive loading is carried by aquatic-subquatic elements, and tree pollen taxa are distributed as in the successive altitudinal/climatic vegetation belts on the western flank of Mount Lebanon (Table 1),

CPD
7, 1511–1566, 2011

from the subalpine, mountainous, upper Mediterranean-temperate belts, to the warmer and drier middle Mediterranean zone (evergreen oaks and pines) lying on the Axis 3 negative side close to δ_c. The low contribution of tree pollen taxa and δ_c to Axis 1 and their distribution along Axis 2 and 3 indicate that the dominant arboreal taxa and δ_c fluctuations are partly independent of the sediment components. Nevertheless, taking arboreal pollen all together, AP % values are correlated with Ca content (r = +0.51) and magnetic susceptibility (r = −0.49). The positive correlation between TOM and detrital elements, and the distance between aquatic-subaquatic plant pollen and TOM in factorial plans 1–2 and 1–3 also shows that, in most samples, TOM is derived from the catchment soil erosion rather than from organic production in the local waterbody.

4 The Yammoûneh record vs. time. Comparison with regional terrestrial records

4.1 Reassessment of our age model

During the relatively well-dated MIS 5.5 and early MIS 1, AP % values reach maximum within carbonate-dominated material around ~125–120 and 11.5–9 ka, respectively (Fig. 9a). These maximum are in phase with, or very close to maximum summer insolation at 34° N (Berger, 1978; Fig. 9b). By analogy, we suggest that other arboreal peaks, which all coincide with increased in situ carbonate production, are also in phase with high summer solar radiation. We thus propose to reajust our time scale by tuning the pollen record to this external parameter (Fig. 9c). The larger age differences between tuned and untuned chonology (Fig. 9d) concern MIS 3 and MIS 7 with maximum values of 11.4 and 8.9 ka, respectively. These differences are primarily attributed to changes in sedimentation rates between dated points. However, according to the tuned age model, the geomagnetic event 1 initially assigned to the Lachamp event falls around 32 ka and would rather represent the Mono Lake event, and the ^{14}C age at 47 ka would be older than the actual age. The following sections are based

CPD
7, 1511–1566, 2011

on corrected (tuned) ages, keeping in mind that this new age model also needs to be confirmed by further age measurements.

4.2 The successive glacial-interglacial stages

We now propose a multi-proxy interpretation of the Yammoûneh record constrained by all indicators. Major changes in sedimentation processes, terrestrial vegetation, and oxygen isotope values (Figs. 5–7) are summarized by some selected proxies plotted versus time using the corrected ages as proposed above, but variations based on our initial age model are super-imposed in the graphs (Figs. 10a–f). Figure 10 also displays the timing of Mediterranean sapropel events, S1 to S9 (Fig. 10g; Emeis et al., 2003; Ziegler et al., 2010). These events are linked to increased freshwater flux from African rivers into the EMS primarily triggered by the strengthening of the African monsoon and orbital precessional cycle (Rohling, 1994; Rossignol-Strick and Paterne, 1999; Rohling et al., 2002; Ziegler et al., 2010). They also coincide with enhanced precipitation over the EMS (Kallel et al., 1997; Bar-Matthews et al., 2000) and surrounding lands (Roberts et al., 2008). Orbital forcing is expressed by eccentricity and summer/winter insolation at 34° N controlled by eccentricity modulated by the precessional cycle (Fig. 10h; Berger, 1978). Marine oxygen Isotope Stages (MIS) reflect global ice volume (Fig. 10i; Martinson et al., 1987).

For each major stage, we point out the major environmental features emerging from the combination of the different proxies from Yammoûneh. We then briefly compare our reconstruction with a few selected records from surrounding regions (Fig. 11). The northeastern Mediterranean areas, which respond to changes in temperature and ice-cover in high northern latitudes by drier/wetter glacial/interglacial climates, are represented by records from Lake Ohrid (a karstic lake in a mountainous area of Albania; Lézine et al., 2010; Fig. 11a) and Tenaghi Phillipon (Macedonia; Tzedakis et al., 1994, 2009; Fig. 11b). The AP % pollen curve from Yammoûneh is plotted for comparison (Fig. 11c). West of the Judean mountains from Israel, effective precipitation always remained high enough to allow continuous speleothem growth (sites 3, 5, 6, Fig. 1). The

CPD
7, 1511–1566, 2011

$\delta^{18}O_{speleothem}$ (δ_{speleo}) fluctuations from Soreq and Peqiin Caves (Fig. 11d) are closely linked to EMS δ_{sw} but, according to Bar-Matthews et al. (2003), the lowest values which fit sapropel events integrate the effect of enhanced inland rainfall. In the rain shadow of the Judean mountains, changes in efficient moisture in the endorheic Dead Sea basin (DSB), which extends from Mount Hermon (MAP >1000 mm) to the Arava Valley (MAP 20 mm), were inferred from lake level fluctuations of the Dead Sea and its predecessors (Waldmann et al., 2010; Fig. 10e) and periods of deposition/non deposition of speleothems in the DSB (e.g., sites 4 and 7, Fig. 1; Vaks et al., 2003, 2006; Lisker et al., 2010; Fig. 11f). At the northern edge of the global subtropical highs, in southern Negev, sporadic wet episodes were evidenced by deposition of speleothems (Vaks et al., 2007, 2010) or travertines (Schwartz et al., 1979; Livnat and Kronfeld, 1985; Enmar, 1999; Waldmann et al., 2010) (Fig. 11g). Simulated North African runoff to the EMS illustrates changes in the monsoon activity (Fig. 11h; Ziegler et al., 2010).

4.2.1 The penultimate interglacial period, MIS 7 (~244–190 ka)

Yammoûneh

MIS 7 is poorly resolved at Yammoûneh, partly because several gaps in core recovery (Fig. 4a). This stage is a period of high in situ carbonate production with major peaks around 240 and 220–215 ka and a minor one around 200 ka. The two first ones coincide with the occurrence of a permanent waterbody at the core site and with the maximum development of arboreal vegetation (junipers indicating wet cool conditions, and temperate oaks). Low $\Delta\delta^{18}O$ values suggest heavy local rainfall; intervals with high δ_c may result from the ^{18}O enrichment of inflowing water by a relatively long water residence time in the permanent waterbody and/or enhanced thermal and rainfall seasonality. These two intervals reflect the highest ($P-E$) balance of the whole profile, and might coincide with sapropel events S9 and S8 (MIS 7.1 and 7.3), in phase with maximum summer insolation and seasonal insolation contrast. Lower effective moisture occurred during late MIS 7, as showed by the disappearance of aquatic-subaquatic

CPD
7, 1511–1566, 2011

plant pollen and an opening of the vegetal cover associated with enhanced detrital input.

Surrounding regions

In northeastern Mediterranean, the development of trees during the warm phases of MIS 7 attest for wet conditions. At Peqiin Cave, periods of low δ_{speleo} of MIS 7.5, 7.3 and 7.1 are contemporaneous with sapropel layers 9 to 7 and suggest enhanced rainfall (Bar-Matthews et al., 2003), in agreement with our record. Conversely, in the DSB, Lake Amora dropped significantly after MIS 8 (Torfstein et al., 2009), reflecting a decrease in available water although some speleothems grew at that time. Sporadic wet pulses occurred in southern Negev.

4.2.2 The penultimate glacial period, MIS 6 (~190–130 ka)

Yammoûneh

MIS 6 (~2950–1850 cm) is represented by silty clays with an interbedded marly layer around 170 ka and progressively enriched in carbonate after 150 ka. The AP % increases, and δ_c shifts to reach the lowest values of the profile at the MIS 6 end. These features reflect an overall increase in efficient moisture but rapid environmental changes are, however, observed. At the base, eolian material prevailed in the sediment when the landscape was predominantly steppic. The development of juniper forests then reflects wetter, cool conditions. At ~175–165 ka (~2450 cm), a remarkable event is evidenced by a narrow peak of carbonate, the reappearance of subaquatic plant pollen indicative of high local water availability, and a juniper decline in favor of temperate deciduous oaks indicating a moderate warming. This event also shows a sharp δ_c enrichment together with a $\Delta\delta^{18}O$ drop, possibly reflecting amplified winter rains and enhanced seasonal rainfall and temperature contrasts. This wet-warm event might coincide with S6, the only sapropel event occurring during a glacial period. After

CPD
7, 1511–1566, 2011

~150 ka (2150 cm), junipers became dominant again under the cold conditions of late MIS 6. Even if mean annual precipitation was low, local efficient moisture remained sufficient to maintain arboreal vegetation, wetlands around the core site and depleted δ_c values when low glacial temperature minimized evaporation.

Surrounding regions

The relatively wet conditions recorded at Yammoûneh contrast with the generally dry climate prevailing in northeastern Mediterranean areas, where open vegetation prevailed. In northwestern Iran, the ~200 ka pollen record from Lake Urmia also indicates steppic to semi-desertic conditions generally harsher than the last glaciation (Djamali et al., 2008). At Soreq and Peqiin caves, two episodes with low δ_{speleo} values occurred around 180 and 160–145 ka, respectively. The first one roughly matches S6 and both coincide with slight increases of African river discharge during peaks of summer insolation. The $\delta^{18}O$ and $\delta^{13}C$ records from Soreq also show that conditions during the entire MIS 6 were cold but never as dry as the last glacial period (Ayalon et al., 2002), in agreement with our record. Wet conditions in the DSB induced a high-stand of Paleolake Amora until its decline from ~145 ka, and speleothem growth. In the Negev Desrt, MIS 6 was generally dry but a long period of speleothem deposition (142–109 ka) started at the end of MIS 6 (Vaks et al., 2010).

4.2.3 The Last interglacial maximum and ensuing interstadial periods (~130–74 ka)

Yammoûneh

The last interglacial maximum, MIS 5.5 (~130–120 ka; ~1850–1680 cm) includes the period of optimal conditions for authigenic carbonate production, culminating at ~124 ka. During the sapropel S5 deposition (~129–121 ka), an abrupt decline of junipers replaced by temperate oaks first indicate a warming. Then, a rapid expansion

CPD
7, 1511–1566, 2011

of mesic Mediterranean forests (evergreen oaks and pines) fingerprints the establishment of a typical Mediterranean climate with wet winters and very warm, dry summers. Local wetlands disappeared. A large negative shift of $\Delta\delta^{18}O$ occurs in phase with a dramatic increase in δ_c values. All proxies show that the peak of MIS 5.5 was a period of strongly seasonal hydrological and thermal contrast, with mean annual effective moisture significantly lower than during MIS 7 and even late MIS 6, possibly due to heavy winter rains concentrated on a few months and a long dry, evaporative warm season inhibiting mountainous and temperate trees. MIS 5.5 corresponds to a major change in Yammoûneh environments: after 130 ka, the cool-wet conditions of MIS 7 and MIS 6 never appeared again.

From ~120 to 75 ka, olive gray silty clay are clearly banded. Each band is underlined by darker layers of sand and/or poorly preserved plant remains. This evokes episodic runoff events reworking terrigenous and eolian material accumulated on the basin slopes and followed by quiet decantation periods. The detrital accumulation is interrupted by an interval enriched in carbonate at ~105–100 ka (1500 cm) and passes progressively to a light gray marl above ~90 ka (1200 cm). Open vegetation tends to replace the tree cover but peaks of arboreal pollen, in phase with carbonate-enriched phases, reflect much wetter conditions than during intervening steppic intervals. These peaks also coincide with sharp δ_c enrichment and a $\Delta^{18}O$ decrease, as for MIS 5.5. The first one is assigned to MIS 5.3 (S4). The second one, similar to MIS 5.5 in its mineral composition and isotope pattern, is attributed to MIS 5.1 (S3).

Surrounding regions

Our Yammoûneh record is in overall agreement with pollen data from southeastern Europe and northwestern Iran. Furthermore, in the karstic lake Ohrid, authigenic calcite precipitated during warm phases, when the karstic system was active and forests developed in the catchment area (Lézine et al., 2010), as at Yammoûneh. At Soreq, the general trend of δ_{speleo} is reversed compared to the Yammoûneh δ_c curve, possibly

CPD
7, 1511–1566, 2011

due to paleolimnological factors affecting the Yammoûneh isotope signal based on ostracods. Bar-Matthews et al. (2003) and Bar-Matthews and Ayalon (2004) have reconstructed paleorainfall $\delta^{18}O$ (δ_P) and paleoprecipitation at MIS 5.5 and MIS 5.1 (coincident with S5 and S3, respectively), using Levantine SST_{alk} data and the present-day relationships between $\delta^{18}O$ of rainwater and the rainfall amount. Calculations suggest very low δ_P around 125 ka and a precipitation amount close to modern during early MIS 5.1, followed by sharp δ_P enrichment and rainfall decrease after sapropel events. Substracting Soreq δ_{speleo} values from δ_{foram} of marine cores MD-9501 and MD 9509 (~90 ka), Almogi-Labin et al. (2009) concluded that smaller than average $\Delta\delta^{18}O_{sea-land}$ ($=\delta_{foram}-\delta_{speleo}$) imply heavy inland rainfall events during sapropel events S3 and S1, in agreement with our observations. Conversely, the DSB conditions remained generally dry: paleolake Samra experienced lowstands during the whole MIS 5 (Waldmann et al., 2009) and no period of speleothem growth was found. Southward, speleothem and travertine deposition occurred in central and southern Negev, especially during MIS 5.5 when the African (Hoelzmann et al., 2004; Ziegler et al., 2010) and Indian monsoons (Fleitmann et al., 2003, 2009) were considerably reinforced.

4.2.4 The last glacial period, MIS 4, 3 and 2 (~970–225 cm, ~74–15 ka)

Yammoûneh

Olive gray clay first prevails and the maximum contribution of eolian dust to sedimentation appears around 70 ka (900 cm). After ~30 ka, the greenish clay passes without transition to strongly oxidized ocher, reddish clayey silt containing limestone gravels and carbonate concretions suggesting frequent desiccations; an increase in carbonate content, mainly detrital, is attributed to physical erosion of the watershed dolomitic limestones in an environment almost devoid of vegetation. Indeed, a step-wise shift to a steppic-desertic landscape is recorded, although two moderate tree pollen peaks reflect short-term humid pulses likely synchronous with those showed from pollen (Langgut, 2008) and isotope data (Almogi-Labin et al., 2009) in cores MD9501 and

CPD
7, 1511–1566, 2011

MD9509. The δ_c increase is consistent with the overall drying trend inferred from pollen. The driest episode of the whole record occurred between ~23 to 15 ka (LGM and Termination 1; MIS 2), when local water availability was considerably reduced. This does not necessarily mean extremely low regional precipitation according to the $\Delta\delta^{18}O$ values, but may reflect water storage in Mount Lebanon glaciers and permafrost in the Mnaïtra plateau when temperature was at least 10 °C lower than today. The last glacial stage experienced a trend toward arid conditions, and clearly differs from MIS 6 which was generally wetter and experienced an overall increase in efficient moisture.

Surrounding regions

In northeastern Mediterranean and northwestern Iran, dry conditions and lower winter temperature than today prevailed during the last glacial cycle. At Lake Ohrid, detrital siliciclastic particles accumulated, while tree pollen percentages felt dramatically in favor of steppic grasses due to strong deficits in available water stored as ice in the mountains (Lézine et al., 2010). At Lake Urmia, sedimentation was also dominated by siliciclastic input from the strongly eroded, poorly vegetated slopes. In caves from western Israel, δ_{speleo} increased, as δ_c at Yammoûneh, suggesting an overall desiccation trend. In contrast, a remarkable increase in effective water took place in the DSB. Paleolake Lisan rose abruptly at the onset of MIS 4 to reach maximum levels at 27–25 ka (Bartov et al., 2003; Bookmann et al., 2006) or 35–17 ka (Lisker et al., 2009) and then dropped drastically to its minimum level (~14 ka). Many speleothem ages reflect much wetter environments than today from 70 to 13 ka in the DSB. In southern Negev, indices of wet events are scarce, although large floods have occurred between 33 and 29 ka probably in response to anomalies in the Red Sea Trough system (Greenbaum et al., 2006).

CPD
7, 1511–1566, 2011

4.2.5 The past 15 ka

Yammoûneh

The rapid re-establishment of humid conditions in the basin, in response to ice melting and enhanced precipitation, is evidenced by, successively, a step-wise decrease in δ_c after ~15 ka, the sudden development of deciduous oaks after 13 ka, and the deposition of a white lacustrine marl rich in rests of aquatic organisms after 11.5 ka. The wetting optimum is reached from ~11 to 8.5 ka, in phase with S1. In the core, the Holocene is truncated at ~7.5 ka, but a trend toward aridity starting at ~7 ka is registered by the isotope record in trench TR02 (Develle et al., 2010).

Surrounding regions

The early Holocene wetting observed at Yammoûneh was clearly evidenced at other sites from northern Levant. In Lebanon, changes in growth rate, $\delta^{18}O$ and $\delta^{13}C$ in a 12 ka speleothem from Jeita Cave (Fig. 1, site 1) show sharp increases in moisture at ~11.2 and ~10.5 ka and a shift toward drier conditions after 6.5 (Verheyden et al., 2008). The Jeita and Yammoûneh $\delta^{18}O$ run parallel (Develle et al., 2010). Similar wet/dry shifts are showed in the ~15 ka-pollen records from the Aammish marsh in the Bakka Plain (Fig. 1, site 2; Hajar et al., 2008, 2010) and from the Ghab Valley in Syria (Yasuda et al., 2000). At Soreq, inferred rainfall amount was higher than today during S1 and felt by steps after 7 ka. A synthesis of lake isotope records show that wetter early Holocene conditions characterize the eastern Mediterranean region and imply increases in local rainfall (Roberts et al., 2008), when vegetation studies highlighted the role of increased seasonal hydrological contrasts (Peyron et al., 2011). Again, the DSB behave differently. The minor positive Holocene oscillations of the Dead Sea (Enzel et al., 2003; Migowski et al., 2006) and Lake Tiberias (Kinneret; Hazan et al., 2005) did not rival those of the preceding glacial periods. Monsoon rainfalls were intense in the northern tropics (Hoelzmann et al., 2004; Fleitmann et al., 2003, 2009).

CPD
7, 1511–1566, 2011

4.3 Discussion

4.3.1 Glacial-interglacial modes

Over the last 250 ka, the Yammoûneh basin, the NE Mediterranean region and the northern tropics experienced conditions wetter than today during interglacial periods, although through different climatic mechanisms and different moisture sources, while the DSB dried. Our record is in general agreement with long terrestrial sequences from the northeastern Mediterranean, except during MIS 6. Shifts from dry to wetter conditions occurred in response to the transition from glacial to interglacial modes, associated with increased summer insolation and major reductions of ice sheets in the North Hemisphere.

The Yammoûneh record reflects changes in air mass trajectories and in seasonal hydrological contrast. During glacial periods, the NH ice sheet extent induced the southward migration of the mid-latitude westerly belt, as showed by data and coupled ocean-atmosphere circulation models for the LGM (e.g., Li and Battisti, 2008 ; Laîné et al., 2009). The influx of moist air masses from the northwest was thus reduced in northern Levant. During Interglacial stages, the pollen record shows a wetting phase followed by a trend toward drier conditions. Similar trends were observed during and after sapropel events in the Soreq Cave isotopic record (Bar-Matthews et al., 2003). These shifts might reflect a change in rainfall seasonality. A shift from winter-only precipitation, with enhanced hydrological contrast, to an higher relative contribution of spring rains was proposed to explain the early-mid Holocene change in vegetation and isotope data from lakes in western Iran (Stevens et al., 2001, 2006) and the mid-Holocene development of deciduous oaks from western Iran to eastern Turkey (Djamali et al., 2010). During MIS 5.5, increased advection of cold continental air from the North and colder temperatures, linked to a high NAO index, occurred in winter over the near East (Felis et al., 2004). However, based on modern data, Vaks et al. (2010) suggest that lower winter temperatures rather indicate a negative NAO index, leading to

CPD
7, 1511–1566, 2011

increased winter precipitation. Both processes may have acted on Lebanese environments, especially on δ_P values. Amplified thermal seasonal cycle due to increased summer insolation have certainly enhanced evapotranspiration and evaporation from the Yammoûneh surface waterbody during the warm dry season, while these factors were minimized in glacial times.

4.3.2 An overall decrease in local efficient water

A step-wise decline in local available moisture is evidenced along the Yammoûneh profile. Episodes of maximum moisture occurred during MIS 7, and MIS 6 was wetter than the late glacial stage. The amplitude of wet pulses decreased from MIS 5.5 to the Holocene onset. The basin infilling by lake sediments might explain the almost total disappearance of permanent waterbodies after 130 ka and frequent desiccation periods during late MIS 3-MIS 2, but not changes in terrestrial vegetation. The long-term aridity trend coincides with a weakening of the seasonal insolation contrasts linked to the decreasing amplitude of the eccentricity cycle. It is as though the Yammoûneh water balance was partly controlled by the intensity of winter cooling and seasonal insolation contrast, and more moderate mean annual water availability during periods of relatively soft winters after ~70 ka.

4.3.3 Relatively wet local conditions during MIS 6

The pollen and carbonate isotope data from Yammoûneh are in line with the $\delta^{18}O$ and $\delta^{13}C$ records from Soreq Cave in showing generally wetter conditions during MIS 6 than during the last glacial period. Higher ecccentricity values may be the cause. MIS 6 is the only stage where the Yammoûneh and the DSB hydrological evolution are roughly in agreement. Having in mind that the influence of the Nile River extent as north as Cyprus in the Levantine basin during S3 and S1 (Almogi-Labin et al., 2009), an indirect tropical influence superimposed to the dominant role of the

CPD
7, 1511–1566, 2011

North Atlantic-Mediterranean system might have been transmited to the western Levant through the EMS realm. The North African runoff events were slightly stronger than during the last glacial phase (Fig. 11h). Another hypothesis is the impact on northern Levant water balance of the extent of the remote Eurasian ice sheet much larger at 160–130 ka than during the LGM (Svenden et al., 2004) and of the resulting huge proglacial lakes over central Europe (Mangerud et al., 2004).

4.3.4 Antiphasing with the Dead Sea basin after 130 ka

Changes in available water at Yammoûneh are clearly out of phase with the DSB lake-level fluctuations after 130 ka. This is surprising due to the short distance that separates northern Lebanon from the Jordan River headwaters. In the complex physiogeographic pattern of the Levant, regional and local factors may result in different hydrological responses to large-scale climatic changes. During Glacials, the southward shift of the major storm-tracks to the south of the Mediterranean Sea may explain lake higstands in the DSB (Begin et al., 2004; Enzel et al., 2008), and a reversed rainfall gradient between northern and southern Levant compared to modern. During interglacials, the subsidence of easterly airflows linked to the reinforced Indian monsoon activity might have been more efficient in the SE Levant, generating aridity in the Dead Sea basin, than in the northwestern part of the region. The regional topography favors the penetration of subtropical southerly air-flows in the narrow, deep DSB corridor, while the small Lebanese basins are open to the north and are more sensitive to northern influence. Local factors and the specific functioning of individual hydrosystems should also be considered. At Yammoûneh, water storage by ice in Mount Lebanon glaciers and frozen soils have reduced the local liquid water availability during the coldest phases. Although glaciers have occurred in Mount Hermon (Magaritz, 1973), the generally lower latitude and altitude of the Jordan Valley have minimized the downstream impact of highland ice storage. At Yammoûneh, rapid infiltration in the aquifer recharge zone and seepage through the lake bottom evaporation

CPD
7, 1511–1566, 2011

effects always reduced the evaporation effects. In the DSB, where local winds predominate on the large-scale wind components, local temperature and related evaporation rates are crucial factors controlling the Dead Sea water balance (Alpert et al., 1997). Over the past decades, the Dead Sea level lowering has decreased the lake breeze which tempers the local hot and dry climate, and enhanced the impact of the westerly Mediterranean breeze (Shafir and Alpert, 2010). When flowing down from the Judean mountains to the Dead Sea, the descent of the Mediterranean breeze speeds up the wind and the adiabatic heating warms and dries the Dead Sea area, inducing lower air humidity and higher evaporation (Shafir and Alpert, 2010). Such a mechanism might have acted during the warm interglacial periods.

5 Conclusions

The 250 ka Yammoûneh record is far to be as accurate as the well-dated, high-resolution speleothem and lake records from Israel, and still suffer chronological uncertainties, especially before 130 ka. Nevertheless, our study represents the first long paleoenvironmental-paleoclimatic reconstruction for the northern Levant. The combination of pollen, sediment properties and isotope data allows us to cross-check the information derived from environmental indicators established independently.

During the warm interglacial periods, efficient moisture was higher than today. The development of forested landscapes, intense groundwater circulation, and reduced differences between the reconstructed isotopic composition of EMS surface water and lake water reflect enhanced precipitation amounts. Wet pulses apparently match EMS sapropel events and phases of high summer insolation, when cool winters and dry warm summers resulted in enhanced seasonal hydrological and thermal contrasts.

CPD
7, 1511–1566, 2011

The driest local conditions established during the last glacial period and culminated during the LGM and the early part of the last deglaciation, when water was probably stored as ice in the surrounding highlands.

The penultimate glacial period was cool by wetter than the last glacial period, possibly due to higher orbital eccentricity values and a stronger but indirect tropical influence, or teleconnections with the remote central Europe.

An overall moisture decrease from MIS 7 to MIS 1 is coincident with a weakening of the seasonal insolation contrast resulting from a long-term eccentricity decline.

Our record roughly agrees with terrestrial records from the NE Mediterranean region (except during MIS 6), and with the western Israel speleothems records when interpreted in terms of rainfall amount. Conversely, after 130 ka, it is clearly out of phase with the hydrological evolution of the Dead Sea Basin. This antiphasing is probably associated with latitudinal migrations of the mid-latitude westerly belt induced by the growth/decay of northern ice sheets. It also suggests that the regional topography, as well as local climatic and hydrological factors, have significantly affected the water availability and the specific behavior of individual hydrosystems.

Further work is required to obtain additional age control points, constrain changes in sedimentation rates, and better determine the timing of observed environmental changes. Acquisition of other long records from northern Levant would be needed to confirm our climatic interpretation. Quantification of paleoclimatic variables should be attempted, and seasonal changes in rainfall and temperature carefully taken into account. We expect that hydrological modeling of the Yammoûneh system will help understand its functioning, and climate modeling will yield better sound hypotheses for explaining the spatial heterogeneity in available moisture in the Levant region.

Acknowledgements. We are grateful to P. Tapponnier, Singapur University, and A. Sursock, CNRG-CNRS-Lebanon, who initiated the investigation of the Yammoûneh basin. We thank colleagues from the IPG-P, from the CNRG, and A. Elias, American University in Beyrouth, for their help during fieldwork and fruitful discussions. Thanks are due to M. Decobert and the SETEL team (CEREGE, CNRS) for coring, to C. Sonzogni (CEREGE), T. Otto and J.-J. Dedoubat (ECOLAB) for technical assistance. L. Lisker, the Hebrew University of Jerusalem

CPD
7, 1511–1566, 2011

and M. Ziegler, Lamont-Doherty Earth Observatory kindly transmit us their data files on DSB-basin speleothems and simulated African river runoff. Financial support came from the CNRS-France, the CNRS-Lebanon, the IPG-P, the French Embassy in Lebanon, the CEDRE French-Lebanese program, and the French project INSU-LEFE-EVE-PALEOLIBAN.

References

Abi-Saleh, B. and Safi, S.: Carte de la végétation du Liban, Ecologia Mediterranea, 14, 123–141, 1988.

Affek, H. P., Bar-Matthews, M., Ayalon, A., Matthews, A., and Eiler, J. M.: Glacial/interglacial temperature variations in Soreq cave speleothems as recorded by "clumped isotope" thermometry, Geochim. Cosmochim. Ac., 72(22), 5351–5360, 2008.

Almogi-Labin, A., Bar-Matthews, M., Shriki, D., Kolosovsky, E., Paterne, M., Schilman, B., Ayalon, A., Aiznshtat, Z., and Matthews, A.: Climatic variability during the last 90 ka on the southern and northern Levantine basin as evident from marine records and speleothems, Quaternary Sci. Rev., 28, 2882–2896, 2009.

Alpert, P., Shafir, H., and Issahary, D.: Recent changes in the climate of the Dead Sea Valley, Climatic Change, 7, 1–25, 1997.

Alpert, P. and Ziv, B.: The Sharav cyclone: observations and some theoretical considerations, J. Geophys. Res., 94, 18495–18514, 1989.

Aouad, A., Travi, Y., Blavoux, B., Job, J. O., and Najem, W.: Etude isotopique de la pluie et de la neige sur le Mont Liban : premiers résultats, Hydrological Sciences, 49, 429–441, 2004.

Aouad, A., Job, J. O., Khalil, S., Touma, T., Bitar, C., Bocquillon, C., and Najem, W.: Snow in Lebanon: a preliminary study of snow cover over Mount Lebanon and a simple snowmelt model, Hydrological Sciences, 50(3), 555–569, 2005.

Ayalon, A., Bar-Matthews, M., and Kaufman, A.: Climatic conditions during marine oxygen isotope 6 in the eastern Mediterranean region from the isotopic composition os speleeothems of Soreq Cave, Israel, Geology, 30, 303–306, doi:10.1130/0091-7613(2002)030<0303:CCDMOI>2.0.CO;2, 2002.

Badertscher, S., Fleitmann, D., Cheng, H., Edwards, R. L., Göktürk, O. M., Zumbühl, A., Leuenberger, M., and Tüysüz, O.: Pleistocene water intrusions from the Mediterranean and Caspian sea into the Black Sea, Nat. Geosci., 4, 236–239, doi:10.1038/NGEO1106, 2011.

CPD
7, 1511–1566, 2011

Bar-Matthews, M. and Ayalon, A.: Speleothems as paleoclimate indicators, a case study from Soreq Cave located in the eastern Mediterranean region, Israel, in Past Climate through Europe and Africa, edited by: Battarbee R. W., Gasse, F., and Stickley, C. S., Springer, Dordrecht, 363–391, 2004.

Bar-Matthews, M., Ayalon, A., and Kaufman, A.: Timing and hydrological conditions of sapropel events in the Eastern Mediterranean, as evident from speleothems, Soreq Cave, Israel, Chem. Geol., 169, 145–156, 2000.

Bar-Matthews, M., Ayalon, A., Gilmour, M., Matthews, A., and Hawkesworth, C. J.: Sea-land oxygen isotopic relationship from planktonic foraminifera and speleothems in the Eastern Mediterranean region and their implication for paleorainfall during interglacial intervals, Geochim. Cosmochim. Ac., 67(17), 3181–3199, 2003.

Bar-Yosef, O.: The Natufian Culture in the Levant, Threshold to the origins of agriculture, Evol. Anthropol., 6, 169–177, 1998.

Bartov, Y., Goldstein, S. L., Stein, M., and Enzel, Y.: Catastrophic arid episodes in the Eastern Mediterranean linked with the North Atlantic Heinrich events, Geology, 31(5), 439–442, 2003.

Begin, Z. B., Stein, M., Katz, A., Machlus, M., Rosenfeld, A., Buchbinder, B., and Bartov, Y.: Southward migration of rain tracks during the last glacial, revealed by salinity gradient in Lake Lisan (Dead Sea rift), Quaternary Sci. Rev., 23, 1627–1636, 2004.

Berger, A. L.: Long-term variations of daily insolation and Quaternary climatic changes, J. Atmos. Sci., 35, 2362–2367, 1978.

Besançon, J.: Le poljé de Yammoûné, Revue Libanaise de Géographie, 3, 3–62, 1968.

Bookman, R., Bartov, Y., Enzel, Y., and Stein, M.: The levels of the late Quaternary lakes in the Dead Sea basin: two centuries of research, in: New Frontiers in Dead Sea Paleoenvironmental Research, edited by: Enzel, Y., Agnon, A., and Stein, M., Geological Society of America Special Paper, 401, 155–170, 2006.

Carto, S., Weaver, A. J., Hetherington, R., Lam, Y., and Wiebe, E. C.: Out of Africa and into an ice age: on the role of global climate change in the late Pleistocene migration of early modern humans out of Africa, J. Hum. Evol., 56, 139–151, 2009.

Castañeda, I., Shefuss, E., Pätzold, J., Sinninghe Damsté, J. S., Weldeab, S., and Schouten, S.: Millenial-scale sea surface temperature changes in the eastern Mediterranean (Nile River Delta region) over the last 27,000 years, Paleoceanography, 25, PA1208, doi:10.1029/2009PA001740, 2010.

CPD
7, 1511–1566, 2011

Craig, H. and Gordon, L. I.: Deuterium and oxygen-18 variations in the ocean and the marine atmosphere, in: Stable Isotopes in Oceanographic Studies and Paleotemperatures, edited by: Tongiorni, E., Consigilio Nazionale delli Ricerche, Laboratorio di Geologia Nucleare, Pisa, 9–130, 1965.

Daëron, M.: Rôle, cinématique et comportement sismique à long terme de la faille de Yammoûneh, principale branche décrochante du coude transpressif libanais (faille du Levant), Unpublished PhD thesis, University Paris 6, 2005.

Daëron, M., Benedetti, L., Tapponnier, P., Sursock, A., and Finkel, R. C.: Constraints on the post-25-ka slip rate of the Yammoûneh fault (Lebanon) using in situ cosmogenic ^{36}Cl dating of offset limestone-clast fans, Earth Planet. Sci. Lett., 227(1–2), 105–119, 2004.

Daëron, M., Klinger, Y., Tapponnier, P., Elias, A., Jacques, E., Sursock, A.: 12,000-year-long record of 10 to 13 paleoearthquakes on the Yammoûneh fault, Levant fault system, Lebanon, B. Seismol. Soc. Ame., 97(3), 749–771, 2007.

Dayan, U., Ziv, B., Shoob, T., and Enzel, Y.: Suspended dust over southeastern Mediterranean and relation to atmospheric circulations, Int. J. Climatolo., 28, 915–924, doi:10.1002/joc.1587, 2008.

Develle, A.-L.: Changement de l'environnement et du climat continental au cours des derniers cycles glaciaires/interglaciaires. Approche sédimentologique, géochimique et magnétique de la séquence lacustre du bassin de Yammoûneh (Liban), Unpublished PhD thesis, University of Aix-Marseille III, 312 pp., 2010.

Develle, A.-L., Herreros, J., Vidal, L., Sursock, and Gasse, F.: Controlling factors on a paleolake oxygen isotope record (Yammoûneh, Lebanon) since the Last Glacial Maximum, Quaternary Sci. Rev., 29(7–8), 865–886, doi:10.1016/j.quascirev.2009.12.005, 2010.

Develle, A. L., Gasse, F., Vidal, L., Williamson, D., Demory, F., Van Campo, E., Ghaleb, N., and Thouveny, N.: A 250 ka sedimentay record from a small karstic lake in the northern Levant (Yammoûneh, Lebanon), Palaeogeogr Palaeocl., 305 , 10–27 doi:10.1016/j.palaeo.2011.02.008, 2011.

Djamali, M., de Beaulieu, J.-L., Shah-hosseini, M., Anrieu-Ponel, V., Ponel, P., Amini, A., Alkani, H., Leroy, S.A.G., Stevens, L., Lahijani, H., Brewer, S.: A late Pleistocene long pollen record from Lake Urmia, NW Iran, Quaternary Res., 69, 413–420, 2008.

Djamali, M., Akhani, H., Andrieu-Ponel, V., Braconnot, P., Brewer, S., de Beaulieu, J.-L., Fleitmann, D., Fleury, J., Gasse, F., Guibal, F., Jackson, S. T., Lézine, A.-M., Médail, F., Ponel, P., Roberts, N., and Stevens, L.: Indian Summer Monsoon variations could have affected

CPD
7, 1511–1566, 2011

the early-Holocene woodland expansion in the Near East, The Holocene, 20(5), 813–820, doi:10.1177/0959683610362813, 2010.
Dubertret, L.: Introduction à la carte géologique au 1/50 000 du Liban, Notes et Mémoires du Moyen-Orient, 13, 345–403, 1975.
Ducassou, E., Capotondi, L., Murat, A., Bernasconi, S. M., Mulder, T., Gonthier, E., Migeon, S., Duprat, J., Giraudeau, J., and Mascle, J.: Multiproxy Late Quaternary stratigraphy of the Nile deep-sea turbidite system. Towards a chronology of deep-sea terrigeneous systems, Sediment. Geol., 200, 1–13, 2007.
El Hakim, M.: Les aquifères karstiques de l'Anti-Liban et du nord de la plaine de la Bekaa: caractéristiques, fonctionnement, évolution et modélisation, d'après l'exemple du système karstique Anjar-Chamsine (Liban), Unpublished PhD thesis, University of Montpellier II, 2005.
Emeis, K. C., Schulz, H., Struck, U., Rossignol-Strick, M., Erlenkeuser, H., Howell, M. W., Kroon, D., Mackensen, A., Ishizuka, S., Oba, T., Sakamoto, T., and Koizumi, I.: Eastern Mediterranean surface water temperatures and $\delta^{18}O$ during deposition of sapropels in the late Quaternary, Paleoceanography, 18(1), 1005, doi:10.1029/2000PA000617, 2003.
Enmar, L.: The travertines in the northern and central Arava. Stratigraphy, petrology and geochemistry, Geological Survery of Israel report A/99, 111 pp., 1999.
Enzel, Y., Amit, R., Dayan, U., Crouvi, O., Kahana, R., Baruch, Z., and Sharon, D.: The climatic and physiographic controls of the eastern Mediterranean over the late Pleistocene climates in the southern Levant and its neighboring deserts, Global Planet. Change, 60, 165–192, 2008.
Enzel, Y., Bookman, R., Sharon, D., Gvirtzman, H., Dayan, U., Baruch, Z., and Stein, M.: Late Holocene climates of the Near East deduced from Dead Sea level variations and modern regional winter rainfall, Quaternary Res., 60(3), 263–373, 2003.
Essallami, L., Sicre, M. A., Kallel, N., Labeyrie, L., and Siani, G.: Hydrological changes in the Mediterranean Sea over the last 30,000 years, Geochem. Geoph. Geosy., 8, Q07002, doi:10.1029/2007GC001587, 2007.
Felis, T., Lohmann, G., Kuhnert, H., Lorenz, S. J., Sholz, D., Pätzold, J., Al-Rousan, S. A., and Al-Moghrabi, S. M.: Increased seasonality in Middle East temperatures during the last interglacial period, Nature, 429, 164–168, 2004.
Fleitmann, D. and Matter, A.: The speleothem record of climate variability in Southern Arabia, C. R., Geosciences, 341, 633–642, 2009.
Fleitmann, D., Burns, S. J., Neff, U., Mangini, A., and Matter, A.: Changing moisture sources

CPD
7, 1511–1566, 2011

over the past 330,000 years in northern Oman from fluid-inclusion evidence in speleothems, Quaternary Res., 60, 223–232, 2003.
Frumkin, A., Bar-Yosef, O., and Schwartz, H. P.: Possible paleohydrological and paleoclimatic effects on hominin migration to and occupation of the Levant between MIS 6 and MIS 4, J. Hum. Evol., 60, 437–451, 2011.
Frumkin, A., Ford, D. C., and Schwarcz, H. P.: Continental oxygen isotopic record of the last 170,000 years in Jerusalem, Quaternary Res., 51(3) 317–327, 1999.
Greenbaum, N., Porat, N., Rhodes, E., and Enzel, Y.: Large floods during late Oxygen Isotope Stage 3, southern Negev desert, Israel, Quaternary Sci. Rev., 25, 704–719, 2006.
Hajar, L., Haïdar-Boustani, M., Khater, C., and Cheddadi, R.: Environmental changes in Lebanon during the Holocene: Man vs. climate impacts, J. Arid Environ., 74, 746–755, 2010.
Hajar, L., Khater, C., and Cheddadi, R.: Vegetation changes during the late Pleistocene and Holocene in Lebanon: a pollen record from the Bekaa Valley, The Holocene, 18(7), 1089–1099, 2008.
Hakim, B.: Recherches hydrologiques et hydrochimiques sur quelques karsts méditerranéens. Liban, Syrie et Maroc. Université Libanaise, Section des Etudes Géographiques II, Beyrouth, 1985.
Hazan, N., Stein, M., Agnon, A., Marco, S., Nadel, D., Negendank, J. F. W., Schwab, M. J., and Neev, D.: The late Quaternary limnological history of Lake Kinneret (Sea of Galilee), Israel, Quaternary Res., 63(1), 60–77, 2005.
Hoelzmann, P., Gasse, F., Dupont, L. M., Salzmann, U., Staubwasser, M., Leuchner, D. C., and Sirocko, F.: Palaeoenvironmental changes in the arid and subarid belt (Sahara-Sahel-Arabian Peninsula) from 150 ka to present, in "Past Climate through Europe and Africa", edited by: Battarbee R. W., Gasse, F., and Stickley, C. S., Springer, Dordrecht, 219–256, 2004.
Imbrie, J., Hays, J. D., Martinson, D. G., McIntyre, A., Mix, A. C., Morley, J. J., Pisias, N. G., Prell, W. L., and Shackeltom, N. J.: The orbital theory of Pleistocene climate. Support from a revised chronology of the marine δ^{18}O record, in: Milankovitch and Climate, edited by: Berger, A., Hays, J., and Imbrie, I., Reidel, Hingham, MA, 269–305, 1984.
Kahana, R., Ziv, B., Enzel, Y., and Dayan, U.: Synoptic climatology of major floods in the Negev desert, Israel, Int. J. Climatol., 22, 867–882, 2002.
Kallel, N., Paterne, M., Duplessy, J.-C., Vergnaud-Grazzini, C., Pujol, C., Labeyrie, L., Arnold, M., Fontugne, M., and Pierre, C.: Enhanced rainfall in the Mediterranean region during the

CPD
7, 1511–1566, 2011

last sapropel event, Oceanol. Acta, 20, 697–712, 1997.
Karam, F.: Climate change and variability in Lebanon: impact on land use and sustainable agriculture development, in: Proceedings of the First Technical Workshop of the "Mediterranean" Component of CLIMAGRI Project on Climate Change and Agriculture, 25–27 September, FAO, Rome, 2002.
Kolodny, Y., Stein, M., and Machlus, M.: Sea-rain-lake relation in the Last Glacial East Mediterranean revealed by δ^{18}O-δ^{13}C in Lake Lisan aragonites, Geochim. Cosmochim. Ac., 69, 4045–4060, 2005.
Kroon, D., Alexandser, I., Little, M., Lourens, L. J., Mattthewson, A., Robertson, A. H. F., and Sakamoto, T.: Oxygen isotope and sapropel stratigraphy in the Eastern Mediterranean during the last 3.2 millions years. Ocean Drilling Program Scientific Results, Volume 160, College Station, Texas, 181–190, 1998.
Kuhlemann, J., Rohling, E. J., Krumrei, I., Kubik, P., Ivy-Ochs, S., and Kucera, M.: Regional synthesis of Mediterranean atmospheric circulation during the Last Glacial Maximum, Science, 231, 1338–1340, 2008.
Laîné, A., Kageyama, M., Salas-Mélia, D., Voldoire, A., Rivière, G., Ramstein, G., Planton, S., Tyteca, S., and Peterschmitt, J. Y.: Northern hemisphere storm tracks during the last glacial maximum in the PMIP2 ocean-atmosphere coupled models: energetic study, seasonal cycle, precipitation, Climate Dynamics, 32, 593–614, doi:10.1007/s00382-008-0391-9, 2008.
Langgut D.: Late Quaternary Palynological Sequences from the Eastern Mediterranean Sea, Israel Geological Survey, Report GSI, 16/08 (Hebrew with English abstract), 2008.
Le Pichon, X. and Gaulier, J. M.: The rotation of Arabia and the Levant fault system, Tectonophysics, 153, 271–294, 1988.
Lézine, A.-M., von Grafenstein, U., Andersen, N., Belchemeri, S., Bordon, A., Caron, B., Cazet, J.-P., Erlenkeuser, H., Fouache, E., Grenier, C., Huntsman-Mapila, P., Huzeau-Mazaudier, D., Manelli, D., Mazaud, A., Robert, C., Sulpizio, R., Tiercelin, J.-J., Zanchetta, G., and Zeqolari, Z.: Lake Ohrid, Albania, provides an exceptional multi-proxy record of environmental changes during the last glacial-interglacial cycle, Palaeogeogr. Palaeocl., 287, 116–127, 2010.
Li, C. and Battisti, D. S.: Reduced Atlantic storminess during the Last Galcial Maximum: evidence from a coupled climate model, J. Climate, 21, 3561–3579, 2008.
Lisker, S., Vaks, A., Bar-Matthews, M., Porat, R., and Frumkin, A.: Stromatolites in caves of the Dead Sea Fault Escarpment: implications to latest Pleistocene lake levels and tectonic

CPD
7, 1511–1566, 2011

subsidence, Quaternary Sci. Rev., 28(1–2), 80–92, 2009.
Lisker, S., Vaks, A., and Bar-Matthews, M.: Late Pleistocene palaeoclimatic and palaeoenvironmental reconstruction of the Dead Sea area (Israel), based on speleothems and cave stromatolites, Quaternary Sci. Rev., 29, 1201–1211, 2010.
Livnat, A. and Fronfeld, J.: Paleoclimatic implications of U-sderies dates for lake sediments and travertines in The Arava Rift Valley, Israel, Quaternary Res., 24, 164–172, 1985.
Magaritz, M.: Precipitation of secondary calcite in glacier areas: carbon and oxygen isotopic composition of calcites from Mt. Hermon, Israel, and the European Alps, Earth Planet. Sci. Lett., 17, 385–390, 1973.
Mangerud, Y., Jakobsson, M., Alexanderson, H., Astakhov, V. I., Clarke, G. K. C., Henriksen, M., Hjort, C., Krinner, G., Lunkka, J., Möller, P., Murray, A., Nikolskaya, O., Saarnisto, M., and Svenden, J. A.: Ice-damned lakes and reroutinh of yje drainage of northern Eurasia during the Last Glaciation, Quaternary Sci. Rev., 23, 1313–1332, 2004.
Martinson, D. G., Pisias, N. G., Hays, J. D., Imbrie, J., Moore Jr., T. C., and Shackleton, N. J.: Age dating and the orbital theory of the Ice Ages: development of a high-resolution 0 to 300,000-year chronostratigraphy, Quaternary Res., 27, 1–29, 1987.
McGarry, S., Bar-Matthews, M., Matthews, A., Vaks, A., Schilman, B., and Ayalon, A.: Constraints on hydrological and paleotemperature variations in the Eastern Mediterranean region in the last 140 ka given by the D values of speleothems fluid inclusions, Quaternary Sci. Rev., 23, 919–934, 2004.
Migowski, C., Stein, M., Prasad, S., Negendank, J. F. W., and Agnon, A.: Holocene climate variability and cultural evolution in the Near East from the Dead Sea sedimentary record, Quaternary Res., 66(3), 421–431, 2006.
Peyron, O., Goring, S., Dormoy,I., Kotthoff, U., Pross, J., de Beaulieu, J.-L., Drescher-Schneider, R., Vannière, B., and Magny, M.: Holocene seasonality changes in the central Mediterranean region reconstructed from the pollen sequences of Lake Accesa (Italy) and Tenaghi Philippon (Greece), The Holocene, 21(1), 131–146, doi:10.1177/0959683610384162, 2011.
Paillard, D., Labeyrie, L., and Yiou, P.: Macintosh program performs term-series analysis, Eos Trans., AGU 77, 379, 1996.
Raible, C. C., Ziv, B., Saaroni, H., and Wild, M.: Winter synoptic-scale variability over the Mediterranean Basin under future climate conditions as simulated by the ECHAM5, Climate Dynamics, 35, 473–488, doi:10.1007/s00382-009-0678-5, 2010.

CPD
7, 1511–1566, 2011

Reimer, P. J., Baillie, M. G. L., Bard, E., Bayliss, A., Beck, J. W., Blackwell, P. G., Bronk Ramsey, C., Buck, C. E., Burr, G., Edwards, R. L., Friedrich, M., Grootes, P. M., Guilderson, T. P., Hajdas, I., Heaton, T. J., Hogg, A. G., Hughen, K. A., Kaiser, K. F., Kromer, B., McCormac, F. G., Manning, S. W., Reimer, R. W., Richards, D. A., Southon, J., Turney, C. S. M., van der Plicht, J., and Weyhenmeyer, C.: INTERCAL09 and marine09 radiocarbon age and calibration curves, 0–50,000 years, Radiocarbon, 51(4), 1111–1150, 2009.

Roberts, N., Jones, M. D., Benkaddour, A., Eastwood, W. J., Filippi, M. L., Frogley, M. R., Lamb, H. F., Leng, M. J., Reed, J. M., Stein, M., Stevens, L., Valero-Garces, B., and Zanchetta, G.: Stable isotope records of Late Quaternary climate and hydrology from Mediterranean lakes: the ISOMED synthesis, Quaternary Sci. Rev., 27(25–26), 2426–2441, 2008.

Rodwell, M. J. and Hopkins, B. J.: Monsoons and the dynamics of deserts, Quarterly Journal of the Royal Meteorological Society, 122, 1385–1404, doi:10.1002/qj.49712253408, 1996.

Rohling, E. J.: Review and new aspects concerning the formation of Mediterranean sapropels, Mar. Geol., 122, 1–28, 1994.

Rohling, E. J., Cane, T. R., Cooke, S., Sprovieri, M., Bouloubassi, I., Emeis, K. C., Schiebel, R., Kroon, D., Jorissen, F. J., Lorre, A., and Kemp, A. E. S.: African monsoon variability during the previous interglacial maximum, Earth Planet. Sci. Lett., 202, 61–75, 2002.

Rossignol-Strick, M. and Paterne, M.: A synthetic pollen record of the eastern Mediterranean sapropels of the last 1 Ma: implication for the time-sacle and formation of sapropels, Mar. Geol., 153, 221–237, 1999.

Rozanski, K.: Isotopes in atmospheric moisture, in: Isotopes in the Water Cycle: Past, Present and Future, a Developing Science, Springer Dordrecht, 291–302, 2005.

Rozanski, K., Araguás-Araguás, L., and Gonfiantini, R.: Isotopic patterns in modern global precipitation, Climate Change in Continental Isotopic Records, Geophysical Monograph 78, American Geophysical Union. Washington D. C, 1–36, 1993.

Schwarz, H. P., Blackwell, B., Goldberg, P., and Marks, A. E.: Uranium series dating of travertine from archeological sites, Nahal Zin, Israel, Nature, 277, 558–560, 1979.

Service Météorologique du Liban: Atlas climatique du Liban, Beirut, Lebanon, 1977.

Shafir, H. and Alpert, P.: Regional and local climatic effects on the Dead-Sea evaporation. Climatic Change, 3–4, 455–468, doi:10.1007/s10584-010-9892-8, 2010.

Sharon, D. and Kutiel, H.: The distribution of rainfall intensity in Israel, its regional and seasonal variations and its climatological evaluation, J. Climatol., 6, 277–291, 1986.

Shea, J. J.: Transitions or turnovers? Climatically-forced extinctions of *Homo sapiens* and

CPD
7, 1511–1566, 2011

Neanderthals in the east Mediterranean Levant, Quaternary Sci. Rev., 27, 2253–2270, 2008.
Stevens, L. R., Wright Jr., H. E., and Ito, E.: Proposed changes in seasonality of climate during the Lateglacial and Holocene at Lake Zeribar, Iran, The Holocene, 11, 747, doi:10.1191/09596830195762, 2001.
Stevens, L. R., Ito, E., Schwalb, A., and Wright Jr., H. E.: Timing of atmospheric precipitation in the Zagros mountains inferred from a multi-proxy record from Lake Mirabad, Iran, Quaternary Res., 66, 494–500, 2006.
Sursock, A. and Gasse, F.: Impact des changements climatiques et de l'activité humaine sur l'environnement au Liban. Report Cedre project, Convention N°03 EnF34/L42, French Embassy in Lebanon and CNRS-Lebanon, Beyrouth, 30 pp., 2005.
Svenden, J. A., Alexanderson, H., Astakhov, V. I., Demidov, I., Dowdeswell, J. A., Funder, S., Gataullin, V., Henriksen, M., Hjort, C.,Houmark-Nielsen, M., Hubberten, H. W., Ingolfsson, O., Jakobsson, M., Kjær, K. H., Larsen, E., Lokrantz, H., Pekka Lunkka, J., Astrid Lysi, A., Mangerud, J., Matiouchkov, A., Murray, A., Möller, P., Niessen, P., Nikolskaya, O., Polyak, L., Saarnisto, M., Siegert, C., Siegert, M., Spielhagen, R. F., and Stein, R.: Late Quaternary ice sheet of northern Eurasia, Quaternary Sci. Rev., 13, 1229–1271, 2004.
Torfstein, A., Haase-Schramm, A., Waldmann, N., Kolodny, Kolodny, Y., and Stein, M.: U-series and oxygen isotope chronology of the mid-Pleistocene Lake Amora (Dead Sea basin)., Geochim. Cosmochim. Ac., 73, 2603–2630, 2009.
Tzedakis, P. C.: Vegetation change through glacial-interglacial cycles: a long pollen sequence perspective, Philosophical Transactions of the Royal Society, B 345, 403–432, 1994.
Tzedakis, P. C., Hooghiemstra, and Pälike, H.: The last 1.35 million yeazrs at Tenaghi Philippon: revised chronolstratigraphy and long-term vegetation trends, Quaternary Sci. Rev., 25, 3416–3430, 2009.
Vaks, A., Bar-Matthews, M., Ayalon, A., Schilman, B., Gilmour, M., Hawkesworth, C. J., Frumkin, A., Kaufman, A., and Matthews, A.: Paleoclimate reconstruction based on the timing of speleothem growth and oxygen and carbon isotope composition in a cave located in the rainshadow in Israel, Quaternary Res., 59, 182–193, 2003.
Vaks, A., Bar-Matthews, M., Ayalon, A., Matthews, A., Frumkin, A., Dayan, U., Halicz, L., Almogi-Labin, A., and Schilman, B.: Paleoclimate and location of the border between Mediterranean climate region and the Saharo-Arabian Desert as revealed by speleothems from the northern Negev Desert, Israel, Earth Planet. Sci. Lett., 249, 384–399, 2006.
Vaks, A., Bar-Matthews, M., Ayalon, A., Matthews, A., Halicz, L., and Frumkin, A.: Desert

CPD
7, 1511–1566, 2011

speleothems reveal climatic window for African exodus of early modern humans, Geology, 35(9), 831–834, 2007.
Vaks, A., Bar-Matthews, M., Matthews, A., Ayalon, A., and Frumkin, A.: Middle-Late Quaternary paleoclimate of northern margins of the Saharan-Arabian Desert: reconstruction from speleothems of Negev Desert, Israel, Quaternary Sci. Rev., 29, 2647–2662, 2010.
Verheyden, S., Nader, F. H., Cheng, H. J., Edwards, L. R., and Swennen, R.: Paleoclimate reconstruction in the Levant region from the geochemistry of a Holocene stalagmite from the Jeita cave, Lebanon, Quaternary Res., 70(3), 368–381, 2008.
Waldmann, N., Stein, M., Ariztegui, D., and Starinsky, A.: Stratigraphy, depositional environments and level reconstructon of the last interglacial Lake Samra in the Dead Sea basin, Quaternary Res., 72, 1–15, 2009.
Waldmann, N., Torfstein, A., and Stein, M.: Northward intrusions of low- and mid-latitude storms across the Saharo-Arabian belt during past interglacials, Geology, 38, 567–570, doi:10.1130/G30654.1, 2010.
Yasuda, Y., Kitagawa, H., and Nakagawa, T.: The earliest record of major anthropogenic deforestation in the Ghab Valley, northwest Syria : a palynological study, Quatern. Int., 73/74, 127–136, 2000.
Ziegler, M., Tuenter, E., and Lourens, L. J.: The precession phase of the boreal summer monsoon as viewed from the eastern Mediterranean (ODP site 968), Quaternary Sci. Rev., 29, 1481–1490, 2010.
Ziv, B., Saaroni, H., and Alpert, P.: The factors governing the summer regime of the eastern Mediterranean, Int. J. Climatol., 24, 1859–1871, 2004.
Ziv, B., Dayan, U., Kuschnir, Y., Roth, C., and Enzel, Y.: Regional and global atmospheric patterns governing rainfall in the southern Levant, Int. J. Climatol., 26, 55–73, doi:10.1016/j.quascirev.2005.07.008, 2006.
Ziv, B., Saaroni, H., Romem, M., Heifetz, E., Harnik, N., and Baharad, A.: Analysis of conveyor belts in winter Mediterranean cyclones, Theor. Appl. Climatol., 99, 441–455, 2010.

CPD
7, 1511–1566, 2011

Table 1. Distribution of the modern vegetation belts in the Yammoûneh area as a function of location, altitude, mean annual precipitation (MAP) and mean annual temperature (MAT). After Abi-Saleh and Safi (1988).

	Altitude (m a.s.l.)	MAP (mm yr^{-1})	MAT (T°C)	Characteristic plant taxa
Western flank of Mt Lebanon				
Lower Mediterranean belt	0–500	> 600	20	*Pistacia, Myrtus. . . .*
Middle Mediterranean belt	500–1000	800–1000	16–18	Evergreen *Quercus*, *Pinus*
Upper Mediterranean belt	1000–1500	> 900 – 1000	15–16	Deciduous *Quercus*
Montane belt	1500–2000	> 1000	10–15	*Cedrus, Abies*
Subalpine belt	> 2000	> 1200	0–5	*Juniperus*
Western flank of Mt Lebanon				
	900–1800	600–800	16–18	Evergreen *Quercus*
	> 1800	> 800		*Juniperus*
Bekaa plain		400		Steppe elements

CPD
7, 1511–1566, 2011

Table 2. Performed analyses on the upper 36 m of core YAM04-C'. Variables included in the PCA are numbered in column 2.

Observations and Analyses	Variables included in PCA		Variable	Nb of analyzed samples	
Main lithofacies types	1	Whitish powdery, sandy carbonate	1		
		Pale gray to pale brown marl	2		
		Yellowish brown to reddish brown silt	3		
		Olive gray silty clay	4		
		Brownish gray silty clay	5		
		Dark brown, peaty or paleosoil-like levels	6		
Sediment composition	2	XRD mineralgy (% weight dry sediment)	Calcite (+ Aragonite: 0–3 %)	160	
	3		Quartz	160	
	4		K-Feldspaths + Plagioclases	160	Same
	5		Dolomite	160	samples
	6		Clay minerals	160	
	7	TOM (% weight dry sediment)		160	
	8	Total magnetic susceptibility (10^{-5} SI)		2417	
	9	XRF Element relative content	Ca	2109	
	10		Si	2109	
	11		Al	2109	
	12		Fe	2109	
	13		Ti	2109	
	14		K	2109	
Pollen analysis	15	Steppic-desertic landscape	*Artemisia* + *Chenopodiaceae* + *Cichoroideae*	225	
	16	Middle Mediterranean zone	*Pinus* + *evergreen Quercus*	225	
	17	Upper Mediterranean zone	Deciduous Quercus	225	
	18	Montane belt	*Cedrus* + *Abies*	225	
	19	Subalpine zone	*Juniperus*	225	
	20	Aquatic + Hydrophilous (% total pollen)	*Myrioplyllus, Potamogeton,* Typha, Cyperaceae, Ranunculus	225	
Carbonate oxygen isotope	21	δ_c derived from ostracod δ^{18}O values		190	
Microscopic observations		Smear slides		250	
		Scanning electron microscope		52	Same
Grain size analysis				52	samples

CPD
7, 1511–1566, 2011

Table 3. Significant simple linear correlation coefficients ($p < 0.001$) between environmental variables from Yammoûneh.

	Ca (rel. cont)	Calcite (+ aragonite)	Quartz	Kaolinite+ smectite+ chlorite	K-Fedspaths + Plagio.	Magnetic Susceptinility	TOM	Al (rel. cont)	Si (rel. cont)	K (rel. cont)	Ti (rel. cont)	Fe (rel. cont)	Deciduous *Quercus*
Calcite (+ aragonite) (%)	0.791												
Quartz (%)	−0.756	−0.970											
Kaolinite+smectite +chlorite (%)	−0.620	−0.674	0.509										
K-Fedspaths + Plagio. (%)	−0.551	−0.807	0.570	0.460									
Magnetic Susceptibility (SI)	−0.607	−0.640	0.663		0.678								
TOM (%wt)	−0.484	−0.411	0.330	0.625		0.526							
Al (rel. cont)	−0.760	−0.728	0.687	0.641	0.602	0.624	0.411						
Si (rel. cont)	−0.754	−0.794	0.787	0.520	0.545	0.661	0.456	0.426					
K (rel. cont)	−0.806	−0.784	0.744	0.640	0.602	0.624	0.592	0.976	0.961				
Ti (rel. cont)	−0.836	−0.812	0.882	0.509	0.587	0.657	0.584	0.927	0.955	0.943			
Fe (rel. cont)	−0.786	−0.732	0.689	0.866	0.528	0.697	0.628	0.868	0.794	0.851	0.828		
Juniperus (%)													
Abies + *Cedrus* (%)													
Deciduous *Quercus* (%)	0.361	0.361	−0.338					−0.342	−0.406	−0.407	−0.392	−0.316	
Everg. *Quercus* + *Pinus* (%)	0.335	0.428	−0.496		−0.410								
Steppic (%)	−0.495	−0.572	0.616		−0.708	0.648		0.387	0.553	0.470	0.578	0.408	−0.674
Aquatic + subaquatic (%)													
δ^{18}O carbonate (PDB ‰)													
AP %	0.51					−0.49							

CPD
7, 1511–1566, 2011

Fig. 1. The Levantine region. Location of the Yammoûneh basin and of sites cited in the text. For terrestrial records, 1: Jeita Cave; 2: Aammish marsh; 3: Peqiin Cave; 4: Ma'ale Efrayim Cave; 5: Soreq Cave; 6: Jerusalem West Cave; 7: Na'chal Ami'az Cave.

CPD
7, 1511–1566, 2011

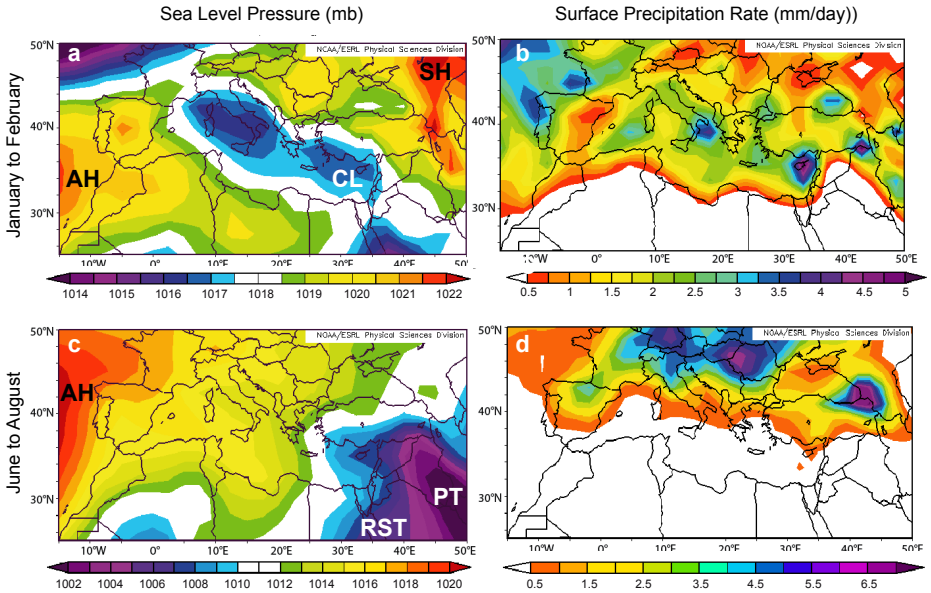

Fig. 2. Sea level pressure and surface precipitation rate in the Mediterranean region in winter (January–February: **a, b**) and summer (June–August; **c, d**) averaged from 1968 to 1996. Source : NCEP /NCAR Reanalysis. NCAA/ESLP Physical Sciences Division (http://www.cdc.noaa.gov/Composites/Day/). AH: Azores High; SH: Siberian High; CL: Cyprus Low; RST: Red Sea Trough; PT: Persian Trough.

CPD
7, 1511–1566, 2011

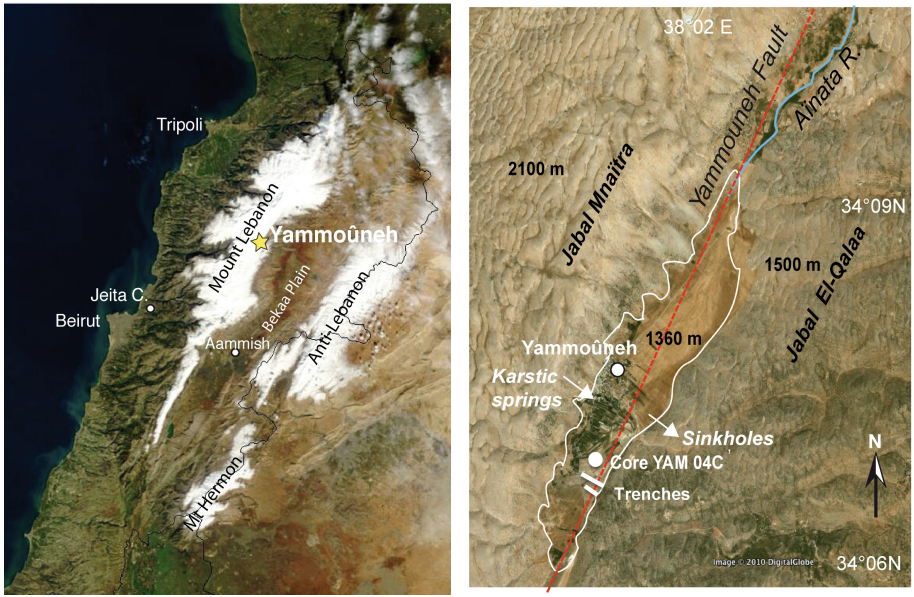

Fig. 3. **(a)** Satellite view of Lebanon in winter (January 2003), main morphological structures. **(b)** The Yammoûneh basin with location of the sedimentary profiles. The red dashed line is the surface trace of the Yammoûneh Fault. Arrows schematize the groundwater circulation, from the Mnaïtra Plateau which provides the main water inflow to the basin via karstic springs emerging along the western edge of the basin, and infiltration along the eastern edge.

CPD
7, 1511–1566, 2011

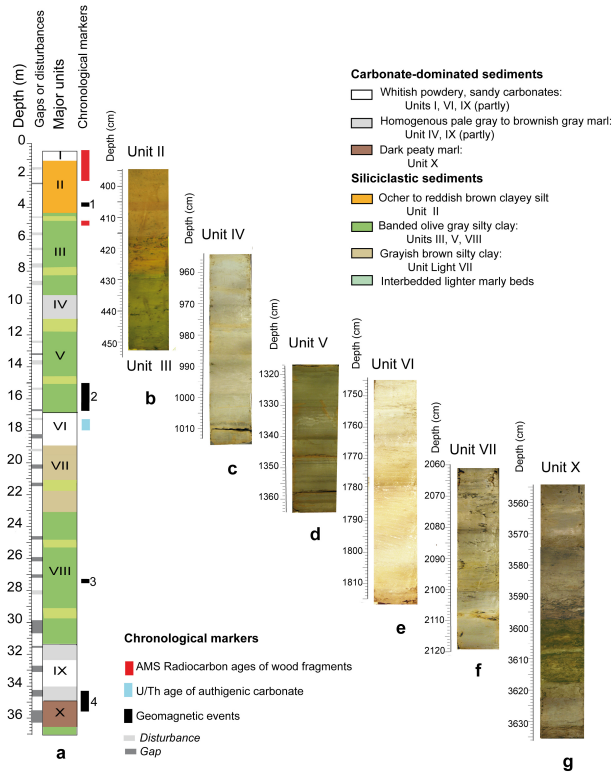

Fig. 4. Major changes in lithofacies along the upper 36 m of core Yam 04 C'. **(a)** Simplified stratigraphic log. The position of gaps in core recovery and sediment disturbances are plotted on the left, that of chronological markers on the right. **(b, g)** Pictures of some core sections illustrating the facies diversity. **(b)** Transition from reddish, oxidized silt of Unit II to olive gray silty clay of Unit III; **(c)** Pale greenish marl; **(d)** Typical banded greenish marl; **(e)** Typical interglacial calcitic powdery deposits; **(f)** Brownish, coarsely banded silty clay; **(g)** Peaty marl of Unit X.

CPD
7, 1511–1566, 2011

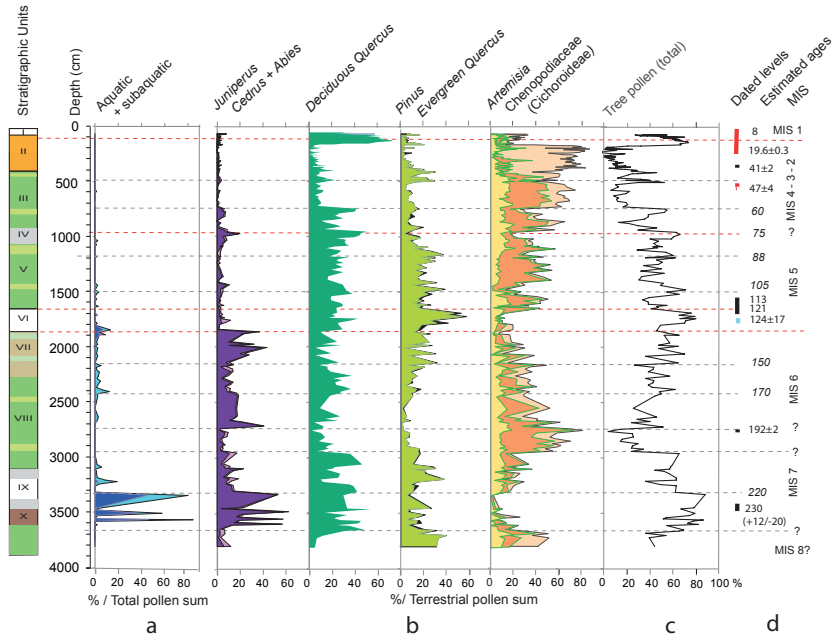

Fig. 5. Paleovegetation. Relative frequencies of main pollen taxa or taxa groups vs. depth along the stratigraphical profile. **(a)** Aquatic and subaquatic plant pollen, expressed in percents of total pollen grains. **(b)** Tree and steppe pollen groups, expressed in percents of terrestrial taxa. **(c)** Total percentages of tree pollen (AP %). After Van Campo et al. (2011). **(d)** Chronological data according to the Develle et al. (2011) age model. Position of the chronological markers (as for Fig. 4), estimated ages of major vegetation changes (in italic, interpolated ages), and Marine oxygen Isotope Stages (MIS; after Martinson et al., 1987). Horizontal dashed lines indicate the major (red) and second order (grey) vegetation changes.

CPD
7, 1511–1566, 2011

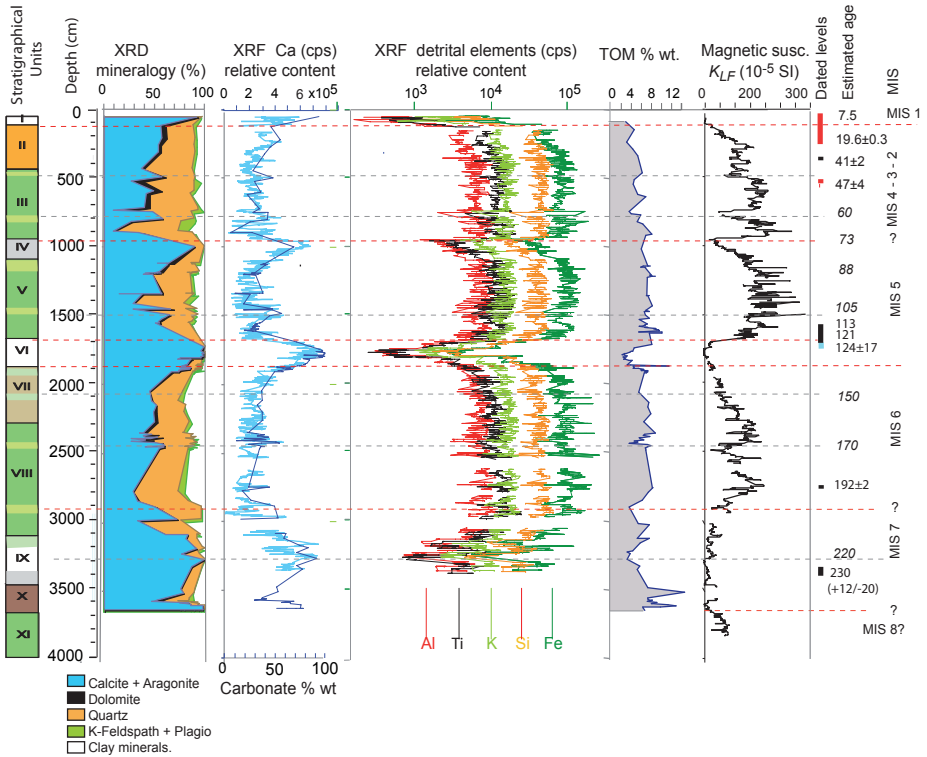

Fig. 6. The sedimentary record. Main sedimentological proxies vs. depth along the stratigraphical profile. After Develle et al. (2011). Horizontal dashed lines indicate the major (red) and second order (grey) sedimentation changes. Chronological data as for Fig. 5d.

CPD
7, 1511–1566, 2011

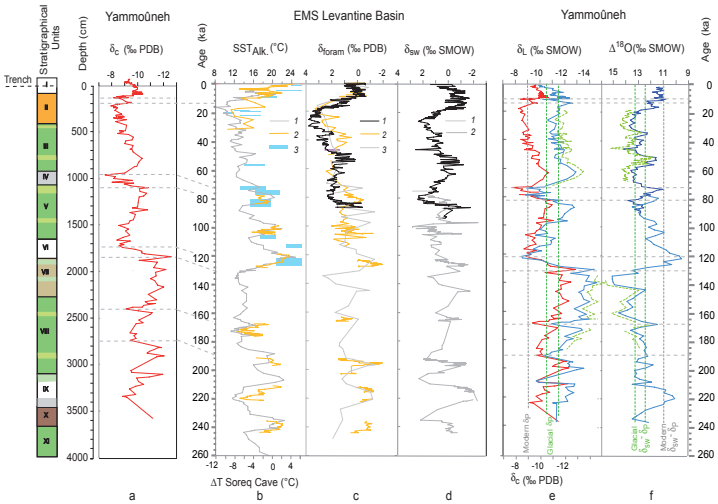

Fig. 7. Carbonate Oxygen isotopes. **(a)** δ_c profile vs. depth (data points above the core top come from trench TR02 where the mid- and late Holocene is preserved). **(b–d)** Times series of marine data used to reconstruct δ_L and $\Delta\delta^{18}O$ versus time. **(b)** Paleo-temperature data. SST_{alk} records from cores M40-71 (1) and ODP 967 (2) (Emeis et al., 2003); for comparison, temperature inferred from $\delta^{18}O$ and δD of fluid inclusions in Soreq Cave speleothems (3, McGarry et al., 2004). **(c)** $\delta^{18}O$ records of planktonic foraminifera (δ_{foram}) from cores MD9501 (1: Almogi-Labin et al., 2009) and ODP 967 (2: Kroon et al., 1998; 3: Emeis et al., 2003). **(d)** Isotopic composition of sea surface water (δ_{sw}) in the Levantine basin inferred from SSTs in core MD40-71 and δ_{foram} from cores MD9501 (1; 0–86 ka) and ODP 967 (2; 78–250 ka). **(e)** δ_c(red) and reconstructed δ_L versus time according to our age model. The blue δ_L curve is based on the modern mean annual temperature difference between sea level and Yammoûneh, the green one account for an additional cooling of 2.5 °C at Yammoûneh during glacial periods. Vertical dashed lines indicate modern and inferred glacial δ_P values. **(f)** Difference between δ_L and δ_{sw}: $\Delta\delta^{18}O = \delta_{sw-} - \delta_L$. Colors as for **(e)**. Vertical dashed lines indicate $\delta_{sw} - \delta_P$ values inferred for modern and glacial times. See text for explanation.

CPD
7, 1511–1566, 2011

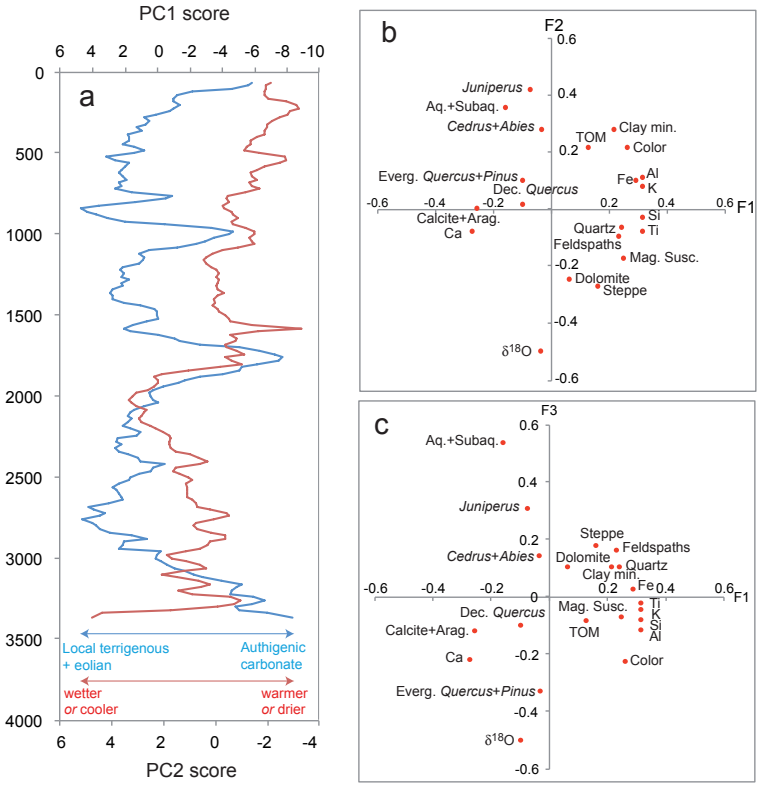

Fig. 8. Principal Component Analysis performed on 21 environmental variables (Table 2) in 157 core levels from core YAM04 C'. **(a)** Scores of the 2 first components (PC1 and PC2) vs. depth. (**b** and **c**) : Projections of environmental variables in the factorial plans F1–F2 and F1–F3, respectively.

CPD
7, 1511–1566, 2011

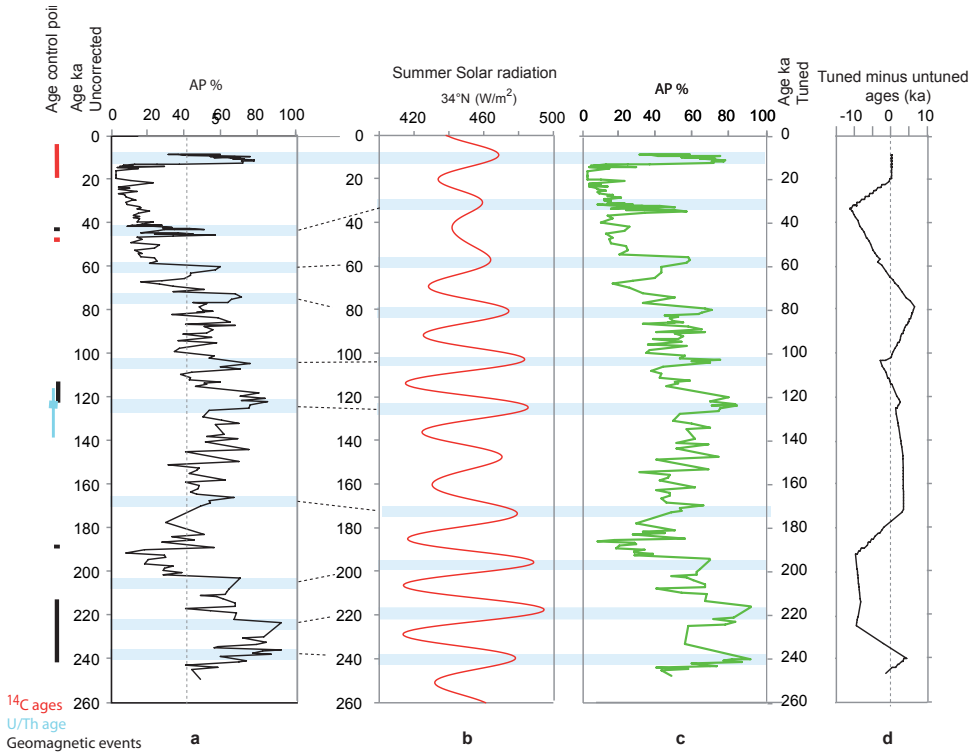

Fig. 9. Correction of our initial age model assuming that all tree pollen peaks are linked to high summer insolation at the Yammoûneh latitude. Age control points used in the initial age model are plotted on the left. **(a)** Arboreal pollen percentages (AP %) relative to total terrestrial pollen vs. time according to our initial age model.**(b)** Summer solar radiation at 34° N (Berger, 1978); **(c)** AP% vs. ages corrected by tuning with summer insolation; **(d)** Age differences between our initial age model and corrected chronology.

CPD
7, 1511–1566, 2011

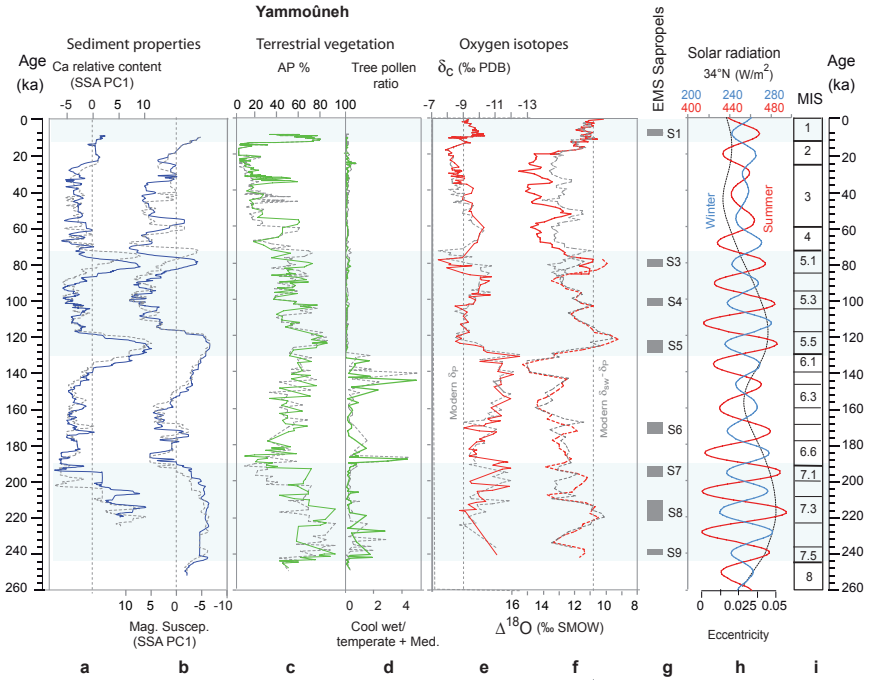

Fig. 10. Major proxies from Yammoûneh versus time **(a, f)**, and potential forcing factors **(g, i)**. Proxy variations according to our initial age model are superimposed in pale gray to those based on corrected ages. **(a)** Ca relative content and **(b)** magnetic susceptibility. For clarity, these two variables are plotted as the first component factor of a Singular Spectrum Analysis (performed using the Paillard et al., 1996, software) and representing 84 and 92.3 % of the total variance, respectively. **(c)** Arboreal pollen percentages relative to total terrestrial pollen (AP %). **(d)** Tree pollen ratio: cool wet forest/(temperate + Mediterranean forest) elements. **(e)** δ_c. **(f)** $\Delta\delta^{18}O$ ($=\delta_{sw}-d_L$; plein curve based on δ_{sw} inferred from core MD9501, dashed curve from core ODP 967). **(g)** Timing of EMS sapropel events (Ziegler et al., 2010). **(h)** Orbital eccentricity and summer/winter insolation at 34° N (Berger, 1978). **(i)** MIS (Martinson et al., 1987).

CPD
7, 1511–1566, 2011

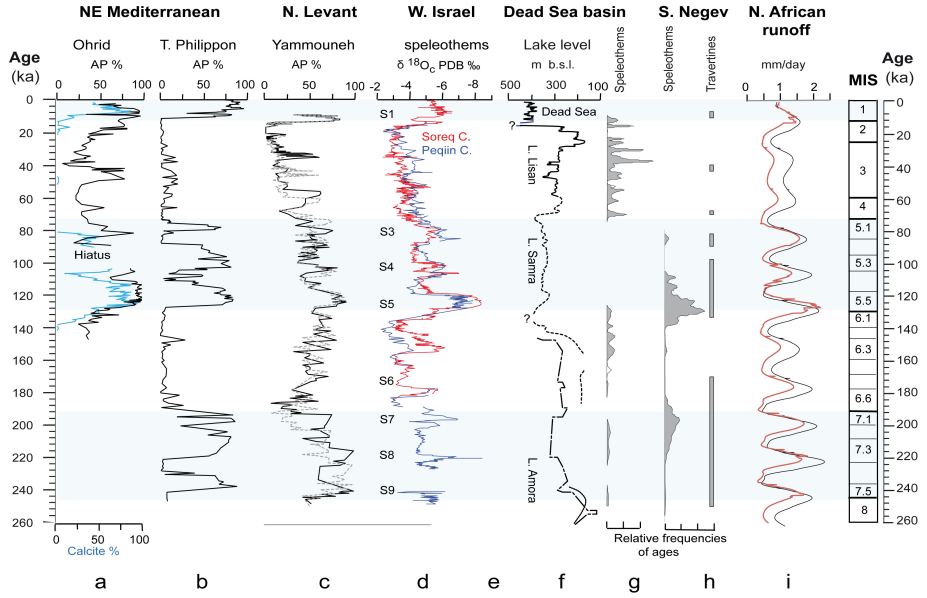

Fig. 11. Some terrestrial regional records from Eastern Mediterranean regions. **(a)** Lake Ohrid, Albania (Lézine et al., 2010); AP % and calcite in % of the mineral assemblage. **(b)** AP % at Tenaghi Philippon, Macedonia (Tzedakis et al., 1994, 2009). **(c)** AP % at Yammoûneh. **(d)** δ^{18}O record from Soreq and Peqiin Caves speleothems, western Israel (Bar-Matthews et al., 2003), and timing of EMS sapropel events (Ziegler et al., 2010). **(e)** Lake level fluctuations of the Dead Sea and its predecessors (Waldmann et al., 2010). **(f)** Relative frequency of ages of speleothem deposition in the Dead Sea basin (Lisker et al., 2010): **(g)** Relative frequency of ages of speleothem deposition in the Negev (Vaks et al., 2010; age frequency is the fraction of speleothems deposited at a certain time with 95 % confidence) and periods of travertine deposition in the Arava valley (Waldmann et al., 2010). **(g)** Simulated North African runoff (Ziegler et al., 2010). Results from the CLIMBER-2 model using orbital forcing only (black curve), orbital forcing + varying NH ice sheets and greenhouse gas concentrations (red curve); **(i)** MIS (Martinson et al., 1987).

CPD
7, 1511–1566, 2011